Practical wavelet design on the sphere

F. Guilloux, G. Faÿ, J.-F. Cardoso

Practical wavelet design on the sphere

Frédéric Guilloux [a,b,c], Gilles Faÿ [a,d,*] and Jean-François Cardoso [a,c].

[a] *AstroParticule et Cosmologie, CNRS and Université Paris 7.*

[b] *Laboratoire Probabilités et Modèles Aléatoires, CNRS and Universités Paris 6-7.*

[c] *Laboratoire du Traitement et de la Communication de l'Information, CNRS and Télécom Paris.*

[d] *Laboratoire Paul-Painlevé, Université Lille-1*

Abstract

We address the question of designing isotropic analysis functions on the sphere which are perfectly limited in the spectral domain and optimally localized in the spatial domain. This work is motivated by the need of localized analysis tools in domains where the data is lying on the sphere, *e.g.* the science of the Cosmic Microwave Background. Our construction is derived from the localized frames introduced by Narcowich et al. (2006). The analysis frames are optimized for given applications and compared numerically using various criteria.

Introduction

Localized analysis for spherical data has motivated many researches during the past decade. Data defined on the sphere are studied in domains as various as cosmology (Hinshaw et al., 2006; Hivon et al., 2002; McEwen et al., 2007), geophysics (Holschneider et al., 2003; Wieczorek and Simons, 2005), medicine, computer vision. When dealing with data on the whole sphere, spectral analysis can be achieved by Spherical Harmonics Transform (SHT) – the equivalent of the Fourier Series on the circle. But in many practical situations, data are defined or available on a subset of the sphere only. For example, cosmologists try to give sharp estimates of the cosmic microwave background (CMB) or its power spectrum but strong foreground emissions superimpose to the CMB making the observations unreliable for CMB studies. Moreover, fully observed

* Corresponding author.
Email address: gilles.fay@univ-lille1.fr (Gilles Faÿ).

clean non stationary fields or stationary fields with additive non-stationary noise still require spatially localized tools. In such situations, the SHT is not adequate, because of the poor spatial localization of the basis functions. In the case of Euclidean spaces, in which the Fourier Transform suffer from the same lack of localization, multiscale and wavelets theory provide a mathematically elegant solution of proven practical efficiency.

Adaptation to the sphere of the "wavelet" transform (in the broad sense of filtering by spatially and spectrally localized functions) was introduced a dozen years ago (Schröder and Sweldens, 1995; Torresani, 1995; Dahlke et al., 1995; Narcowich and Ward, 1996; Potts and Tasche, 1995; Freeden and Windheuser, 1997). Since then, Antoine & Vandergheynst (1999) showed that any Continuous Wavelet Transform (CWT) on the sphere can be viewed locally as a regular CWT on the Euclidean tangent planes, thanks to the stereographic correspondence between the sphere and the plane (Antoine and Vandergheynst, 1999; Wiaux et al., 2005). One can then "forget" the sphere by projecting it on tangent planes, realizing the analysis in these planes, and then apply the inverse projection to get back eventually to the sphere. A discretized version of this approach of CWT has been presented by Bogdanova et al. (2005), leading to wavelet frames. This approach has already been followed in astrophysics for the analysis of the Cosmic Microwave Background (CMB) (Vielva et al., 2004; McEwen et al., 2007). However these wavelets are usually defined in the spatial domain and have infinite support in the frequency domain (which must be truncated in practice).

In the present work, we follow and extend the approach of Narcowich et al. (2006) and their construction of "needlets". A similar construction can be found in Starck et al. (2006). The needlet transform has important characteristics. Firstly it is intrinsically spherical. No intermediate tangent plane is needed to define it. Secondly, it does not depend on the particular spherical pixelization chosen to describe the data. Thirdly, although the needlets still have an excellent spatial localization, they have a finite spectral support adjustable at will . They are axisymmetric (which is convenient when dealing with statistically isotropic random fields) and thus the needlet coefficients are easily computed in the Spherical Harmonics (Fourier) domain. Data filtering is defined by multiplication of the Spherical Harmonics coefficients by well chosen window functions (which is equivalent to convolution in spatial domain). Needlets are well defined in theory and the statistical properties of their coefficients have already been established for isotropic Gaussian fields (Baldi et al. (2006)). However, the performance of a needlet-based analysis depends on the particular shape of the needlet.

This paper considers spherical filters which are generalizations of needlets in the spirit of dual (non-tight) analysis and reconstruction frames. We focus on the design issue, namely the optimization of the window functions (that

define the isotropic filtering operations) for some given tasks. We consider only band-limited needlets. This choice is motivated by applications in high-precision cosmology. Indeed, the CMB power spectrum is highly dynamic (few peaks and power-law decay) and good subsequent cosmological parameters estimation requires high accuracy in some critically delimited spectral ranges. Once the range is fixed, we optimize the shape of window functions in two directions: 1) By requesting the best spatial localization of associated needlets, in an energy-sense ($\mathbb{L}^2$) which is easily solved. This is an application of the work of Simons et al. (2006) which adapted to the sphere the problem solved by Slepian (1978) on the real line, giving rise to the well known prolate spheroidal wave functions (PSWF). 2) By following statistical considerations: given some region ("mask") in which the data is missing or thrown away and assuming that the full data is the realization of some Gaussian isotropic random field (this is the usual assumption made on the CMB), we minimize the mean integrated square error due to the mask in the needlet analysis outside the mask. More criteria and applications to cosmological science will be given in a future work.

The paper is organised as follows. In Section 1, we expose the general construction of needlets. In Section 2, we define and optimize the two criteria (geometrical and statistical) which provide localized analysis filters. Their efficiency is illustrated in Section 3 with numerical simulations following the model of a masked observation of the CMB. The proofs are postponed to Appendix A.

1 Needlets frames

1.1 Background and notations

Denote $\mathbb{S}$ the unit sphere in $\mathbb{R}^3$ with generic element $\xi = (\theta, \varphi)$ in spherical polar coordinates: $\theta \in [0, \pi]$ is the colatitude and $\varphi \in [0, 2\pi[$ the longitude. Let $\mathbb{H} = \mathbb{L}^2(\mathbb{S})$ be the space of complex-valued square integrable functions on $\mathbb{S}$ under the Lebesgue measure $\mathrm{d}\xi = \sin\theta \mathrm{d}\theta\mathrm{d}\varphi$. Endowed with the inner product $\langle f, g\rangle := \int_{\mathbb{S}} f(\xi)g^*(\xi)\mathrm{d}\xi$, $\mathbb{H}$ is a Hilbert space. Let $\|\cdot\|$ denote the associated norm on $\mathbb{H}$. The usual complex spherical harmonics on $\mathbb{S}$ (which definition is recalled in Appendix B) are denoted $(Y_{\ell m})_{\ell\geq 0, -\ell\leq m\leq \ell}$. They form an orthonormal basis of $\mathbb{H}$.

In the following, we consider a field $X \in \mathbb{H}$. Its random spherical harmonics coefficients or multipole moments are denoted $a_{\ell m} = \langle X, Y_{\ell m}\rangle$. $\mathbb{H}$ can be decomposed in harmonic subspaces: $\mathbb{H} = \overset{\perp}{\bigoplus_{\ell\geq 0}} \mathbb{H}_\ell$, where $\mathbb{H}_\ell$ is the linear span

of $Y_{\ell m}, m = -\ell, \cdots, \ell$. The number ℓ is referred to as the multipole number or frequency (understood as a spatial frequency). Let Π_ℓ be the orthogonal projection on $\mathbb{H}_\ell$. It has an expression involving Legendre polynomials L_ℓ (see Appendix B)

$$\Pi_\ell X(\xi) = \sum_{m=-\ell}^{\ell} \langle X, Y_{\ell m} \rangle Y_{\ell m}(\xi) = \int_{\mathbb{S}} X(\xi') L_\ell(\xi \cdot \xi') \mathrm{d}\xi'. \tag{1}$$

where $\xi \cdot \xi' = \cos\theta \cos\theta' + \sin\theta \sin\theta' \cos(\varphi - \varphi')$ is the usual dot product on $\mathbb{S}$.

A mapping on $\mathbb{S}$ which depends on the colatitude θ only is said to be axisymmetric. The convolution of a bounded axisymmetric function $H(\xi) = h(\cos\theta)$ with an arbitrary spherical function X is well defined through

$$H * X(\xi) = \int_{\mathbb{S}} h(\xi \cdot \xi') X(\xi') \mathrm{d}\xi' \tag{2}$$

The convolution theorem holds:

$$H * X = \sum_{\ell m} h_\ell a_{\ell m} Y_{\ell m}. \tag{3}$$

where $a_{\ell m} = \langle X, Y_{\ell m} \rangle$ are the multipole moments of X and h_ℓ are the Legendre series coefficients of h, *i.e.*$h = \sum_{\ell \in \mathbb{N}} h_\ell L_\ell$. Then, an isotropic wavelet analysis can be implemented either in the spatial (*i.e.* direct) domain using (2) or in the harmonic domain using (3). We choose the latter, which accounts to multiply the harmonic coefficients of the field of interest X by a spectral window (h_ℓ). For a countable index set $\mathcal{J}$, let $(h^{(j)})_{j \in \mathcal{J}}$ be a family of window functions in harmonic domain : $h^{(j)} \in \ell^\infty(\mathbb{N})$. The corresponding harmonic smoothing operators on $\mathbb{H}$ are

$$\Psi^{(j)} = \sum_{\ell \in \mathbb{N}} h_\ell^{(j)} \Pi_\ell. \tag{4}$$

We call *exact reconstruction condition* the one ensuring that $\sum_{j \in \mathcal{J}} \Psi^{(j)} = \mathbf{Id}$. It also writes

$$\sum_{j \in \mathcal{J}} h^{(j)} \equiv 1 \tag{5}$$

In the following, j is referred to as the *scale*, in analogy with the multiresolution analysis terminology. Important examples of windows families having the property (5) may be obtained thanks to the B-adic mechanism: let $B > 1$, $\mathcal{J} = \{-1\} \cup \mathbb{N}$, $h_\ell^{(-1)} = \delta_0(\ell)$ and the spectral windows be all related to a continuous function h by

$$\forall j \in \mathbb{N},\ h_\ell^{(j)} = \mathsf{h}\left(\frac{\ell}{B^j}\right). \tag{6}$$

If h is compactly supported on $[\frac{1}{B}, B]$, then each window $h^{(j)}$ may overlap with adjacent windows $h^{(j-1)}$ and $h^{(j+1)}$ only. The exact reconstruction condition in this case is satisfied as soon as

$$\forall x \in [1, B],\ \mathsf{h}(x) + \mathsf{h}(B^{-1}x) = 1 \tag{7}$$

This example is illustrated in Figures 1 and 2.

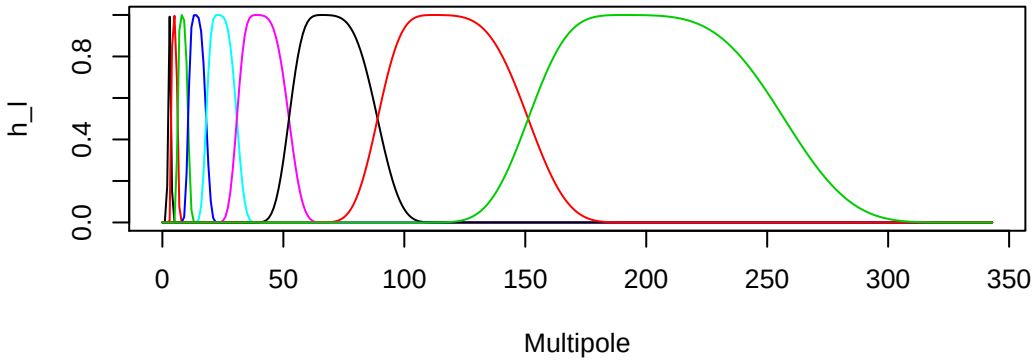

Fig. 1. First 10 windows satisfying conditions (5) and (6), h being a spline of order 7 compactly supported on $[\frac{1}{B}, B]$ with $B = 1.7$.

1.2 Needlet tight frames

Recall that a countable family of functions $\{f_n\}$ in a Hilbert space $\mathcal{H}$ is a frame with frame bounds C_1, C_2 if

$$\forall g \in \mathcal{H}\ ,\ C_1\|g\|_{\mathcal{H}}^2 \leq \sum_n |\langle g, f_n\rangle_{\mathcal{H}}|^2 \leq C_2\|g\|_{\mathcal{H}}^2\ .$$

It is a tight frame if we can choose $C_1 = C_2$. Frames can be thought of redundant "bases", and this redundancy can be exploited for robustness issues. The tightness property is valuable in terms of numerical stability (see Daubechies, 1992, Chap.3 and the references therein).

The construction that follows is from Narcowich et al. (2006). The term *needlet* was coined by Baldi et al. (2006). Let K be a finite index set and $\{\xi_k\}_{k\in K} \in \mathbb{S}^{|K|}$ a set of quadrature points on the sphere, associated with a set $\{\lambda_k\}_{k\in K} \in \mathbb{R}^{|K|}$ of quadrature weights.

Definition 1.1 (Quadrature) *$\{(\xi_k, \lambda_k)\}_{k\in K}$ is said to provide an exact Gauss quadrature formula at degree $\ell_{\max}$ if*

$$\forall X \in \bigoplus_{\ell=0}^{\ell_{\max}} \mathbb{H}_\ell,\ \int_{\mathbb{S}} X(\xi)\mathrm{d}\xi = \sum_{k\in K} \lambda_k X(\xi_k).$$

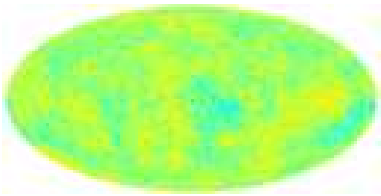

(a) Original map

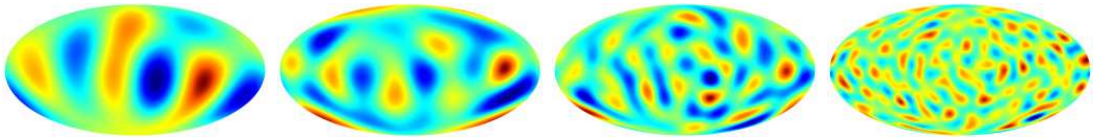

(b) Smoothed maps, scales $j = 2, ..., 5$

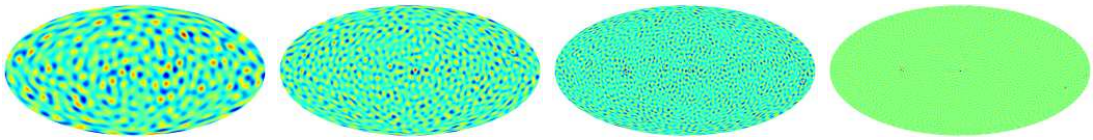

(c) Smoothed maps, scales $j = 6, ..., 9$

Fig. 2. Input map of a CMB sky (from WMAP), and corresponding smoothed maps (with the spline filters of Figure 1).

This quadrature formula is said positive-weight if $\lambda_k > 0, k \in K$.

Remark 1.2 *We refer to Doroshkevich et al. (2005) for an example of a proper choice of quadrature points and weights that fulfils this property (called GLESP). Other pixelization schemes such as HEALPix (Górski et al., 2005) fulfil approximately this property with a number of points of order* $C\ell_{\max}^2$ *and quadrature weights of order* $\frac{1}{C\ell_{\max}^2}$ *for some positive constant* C.

Suppose that the window functions $h^{(j)}$ are non-negative and with finite spectral support. Define

$$\forall \ell \in \mathbb{N},\ b_\ell^{(j)} := \sqrt{h_\ell^{(j)}} \tag{8}$$

and $d^{(j)} := \max\{\ell : h_\ell^{(j)} \neq 0\}$ (in the B-adic case, $d^{(j)} = B^{j+1}$). For each scale j, we have a pixellization $\{\xi_k^{(j)}, \lambda_k^{(j)}\}_{k \in K^{(j)}}$.

Definition 1.3 (Needlets and Needlet coefficients) *For every* $j \in \mathcal{J}$ *and every index* $k \in K^{(j)}$ *the function*

$$\psi_k^{(j)}(\xi) = \sqrt{\lambda_k^{(j)}} \sum_{\ell=0}^{d^{(j)}} b_\ell^{(j)} L_\ell(\xi \cdot \xi_k^{(j)}), \tag{9}$$

is called a needlet. *For $X \in \mathbb{H}$, the inner products $\langle X, \psi_k^{(j)} \rangle$ are called* needlet coefficients *and are denoted $\beta_k^{(j)}$.*

Up to a rotation of the sphere putting $\xi_k^{(j)}$ on the North pole and to the multiplicative term $\sqrt{\lambda_k^{(j)}}$, all the needlets of a given scale j have exactly the same shape. In particular, they are axisymmetric. When $\ell \mapsto b_\ell^{(j)}$ is sufficiently smooth, one gets the intuition from (9) that the needlet $\psi_k^{(j)}$ is localized around $\xi_k^{(j)}$.

The following Proposition state that the harmonic smoothing operation defined by (4) can be seen as the decomposition of $\mathbb{H}$ on the needlets family built with (8), and that this family is a tight frame. It is a straightforward adaptation of Baldi et al. (2006, Proposition 2.3).

Proposition 1.4 *Let $j \in \mathcal{J}$. Assume that $\{(\xi_k^{(j)}, \lambda_k^{(j)})\}_{k \in K^{(j)}}$ provides an exact and positive-weight quadrature formula at degree $2d^{(j)}$. Then*

$$\Psi^{(j)} X = \sum_{k \in K^{(j)}} \beta_k^{(j)} \psi_k^{(j)}.$$

Assume that for any $j \in \mathcal{J}$, $\{(\xi_k^{(j)}, \lambda_k^{(j)})\}_{k \in K^{(j)}}$ provides an exact and positive-weight quadrature formula at degree $2d^{(j)}$. Under the exact reconstruction condition (5),

$$\forall X \in \mathbb{H},\ X = \sum_{j \in \mathcal{J}} \sum_{k \in K^{(j)}} \beta_k^{(j)} \psi_k^{(j)} \quad \textit{and} \quad \|X\|^2 = \sum_{j \in \mathcal{J}} \sum_{k \in K^{(j)}} |\beta_k^{(j)}|^2 \,.$$

Remark on Terminology The analysis of an input field X in the way described above is called *filtering*. This filtering has two equivalent expressions, in the spatial and in the spectral domains; see the convolution formula (3). These expressions involves two "dual" mathematical objects : the functions $h^{(j)}$ and $b^{(j)}$ of the frequency ℓ, called *window functions* or *spectral windows*, and the spherical functions $\psi_k^{(j)}$ called *needlets*, which are nothing else but the rotated axisymmetric functions built from the Legendre transform of $b^{(j)}$ (see Definition 1.3). We call *filter* either of the two above objects, when the domain (spatial or spectral) is not specified.

1.3 Generalized needlet frames

We are concerned with the development of a flexible spectral analysis on the sphere which remains practical at high resolution. The forecoming CMB ex-

periment *Planck* [1] will provide 50 mega-pixel maps with accuracy such that multipole moments will be reliable up to $\ell \simeq 4000$.

For maximum flexibility, we shall consider constructions which are not necessarily dyadic nor B-adic. This is motivated by applications, as described in the Introduction. Moreover, we will design analysis frames which will not be necessarily tight. Their dual frames will be the corresponding reconstruction frames. This allows fine tuning of the localization properties of the decomposition functions but it is also well known that it does not ensure similar properties for the reconstruction functions. Nevertheless, for the application goals discussed in the introduction, we will design strictly band-limited needlets with support $L^{(j)} := [\ell_{\min}^{(j)}, \ell_{\max}^{(j)}]$, $\ell_{\min}^{(j)} > 0$ if $j \geq 0$. Then the subsequent "wavelet design" operations will be performed in the harmonic domain.

Since the needlet coefficients $\beta_k^{(j)}$ and $\beta_{k'}^{(j')}$ of a Gaussian stationary (*i.e.* isotropic) field are independent if $L^{(j)} \cap L^{(j')} = \emptyset$, the bands $L^{(j)}$ are chosen to overlap as little as possible. Other choices are possible; for instance Starck et al. (2006) take overlapping spectral windows supported on $[0, 2^j]$.

The three ingredients for our spherical "multi-resolution" approach are harmonic-space implementation, dual wavelet frames and spectral window design. In this subsection, we briefly describe the first two elements. In Section 2, we go into the theory and practice of window design.

1.3.1 Dual frames

Proposition 1.4 shows that the needlets of Definition 1.3 with (8) can be used in both analysis (or decomposition) and synthesis (or reconstruction). This accounts to say that the needlet frame is its own dual frame. We choose to keep the Definition 1.3 of the needlets and associated coefficients but to relax condition (8). By sacrificing the tightness of the frame, we gain much freedom in the design of the spectral windows. Also, the precise space-frequency picture provided by the needlet construction is preserved.

From any windows family $(b^{(j)})_{j\in\mathcal{J}}$ such that $\forall \ell \in \mathbb{N}, \sum_{j\in\mathcal{J}} \left(b_\ell^{(j)}\right)^2 > 0$, define the synthesis windows $\tilde{b}^{(j)}$ by

$$\forall j \in \mathcal{J},\ \forall \ell \in \mathbb{N},\ \tilde{b}_\ell^{(j)} = \frac{b_\ell^{(j)}}{\sum_{j'\in\mathcal{J}} \left(b_\ell^{(j')}\right)^2} \tag{10}$$

and put $h^{(j)} := \tilde{b}^{(j)} b^{(j)}$ so that (5) easily follows. We retain Definition 1.3 for the *decomposition* needlets and needlets coefficients and further define the

[1] see `www.rssd.esa.int/Planck/`.

reconstruction needlets as

$$\tilde{\psi}_k^{(j)}(\xi) = \sqrt{\lambda_k^{(j)}} \sum_{\ell=0}^{d^{(j)}} \tilde{b}_\ell^{(j)} L_\ell(\xi \cdot \xi_k^{(j)}) \ . \tag{11}$$

Proposition 1.5 *Assume that there exists positive constants C_1, C_2 such that*

$$\forall \ell \in \mathbb{N}, C_1 \leq \sum_{j \in \mathcal{J}} |b_\ell^{(j)}|^2 \leq C_2 \ . \tag{12}$$

Assume that for any $j \in \mathcal{J}$, the set $\{(\xi_k^{(j)}, \lambda_k^{(j)})\}_{k \in K^{(j)}}$ provides an exact and positive-weight quadrature formula at degree $2d^{(j)}$. Then, under the exact reconstruction condition (5), the family $\{\psi_k^{(j)}\}$ is a frame with frame bounds constant C_1 and C_2. Its dual frame is the family $\{\tilde{\psi}_k^{(j)}\}$. In particular

$$\forall X \in \mathbb{H},\ X \overset{\mathbb{H}}{=} \sum_{j \in \mathcal{J}} \sum_{k \in K^{(j)}} \beta_k^{(j)} \tilde{\psi}_k^{(j)} \quad \textit{and} \quad \|X\|^2 = \sum_{j \in \mathcal{J}} \sum_{k \in K^{(j)}} \tilde{\beta}_k^{(j)} \beta_k^{(j)} \ , \tag{13}$$

with $\tilde{\beta}_k^{(j)} := \langle X, \tilde{\psi}_k^{(j)} \rangle$.

Define the analysis, synthesis and smoothing operators at scale $j \in \mathcal{J}$ by $\Phi^{(j)} = \sum_\ell b_\ell^{(j)} \Pi_\ell$, $\tilde{\Phi}^{(j)} = \sum_\ell \tilde{b}_\ell^{(j)} \Pi_\ell$ and $\Psi^{(j)} = \tilde{\Phi}^{(j)} \Phi^{(j)}$, respectively. Then, the exact reconstruction formula $\sum \Psi^{(j)} = \mathrm{Id}$ holds true.

An example of an analysis/synthesis windows family following this scheme is displayed in Figure 3, in which we took optimally concentrated PSWF (see Section 2) functions for analysis. It illustrates the fact that this choice does not lead to well localized synthesis needlets (as their spectral shapes are non smooth). However, this may not be a shortcoming if one is interested in the needlet coefficients $\beta_k^{(j)} = \langle X, \psi_k^{(j)} \rangle$ *per se*, which reflect the local properties of the field X.

1.3.2 Practical computation of needlet coefficients

Evaluation of inner products $\langle X, \psi_k^{(j)} \rangle$ in the direct space is practically unfeasible from a pixelized sphere at high resolutions. The needlet coefficients $\beta_k^{(j)}$ are thus computed via direct and inverse harmonic transforms as a consequence of the following Proposition.

Proposition 1.6 *The needlet coefficients verify $\beta_k^{(j)} = \sqrt{\lambda_k^{(j)}} \Phi^{(j)} X(\xi_k^{(j)})$.*

The computation of the smoothed field $\Phi^{(j)} X$ is performed in the harmonic domain by multiplying the multipole coefficients $a_{\ell m}$ of X by the factors $b_\ell^{(j)}$. Finally, the needlet coefficients $\beta_k^{(j)}$ are retrieved as the values of $\Phi^{(j)} X$ at the

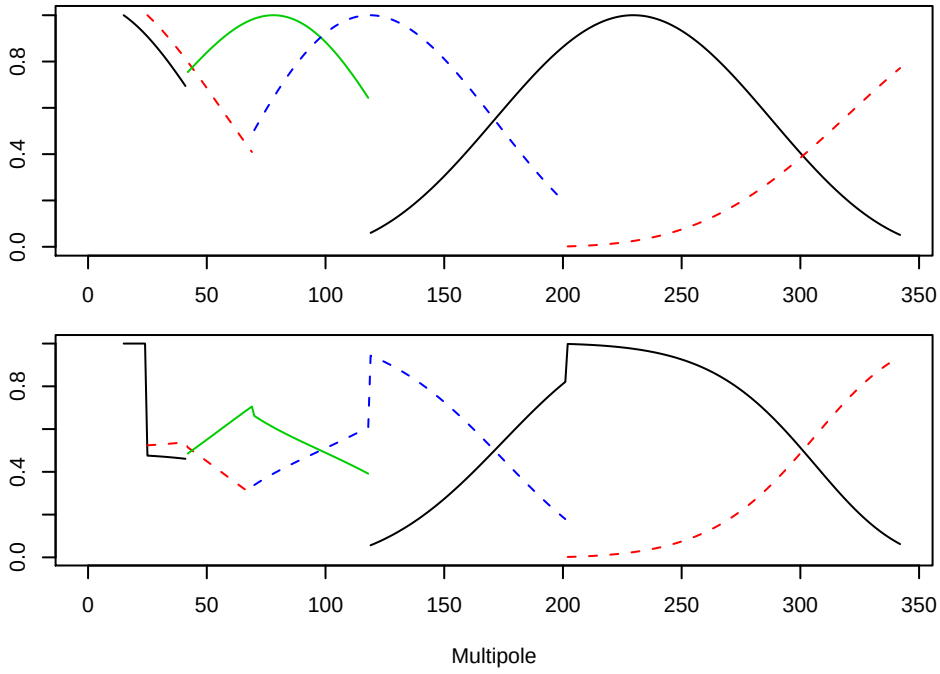

Fig. 3. B-adic analysis (top) and corresponding synthesis (bottom) window functions ($j = 6, \ldots, 11$; $B = 1.7$).

points $\xi_k^{(j)}$ up to a multiplicative term. Starting from the field X sampled at some quadrature points, this operation is summed up by the diagram

$$\{X(\xi_k)\}_{k\in K} \xrightarrow{\text{SHT}} \{a_{\ell m}\}_{\ell m} \xrightarrow{\times} \{b_\ell^{(j)} a_{\ell m}\}_{\ell m} \xrightarrow{\text{SHT}^{-1}} \left\{(\lambda_k^{(j)})^{-1/2}\beta_k^{(j)}\right\}_{k\in K^{(j)}} \quad (14)$$

whereas the synthesis operation is summed up by

$$\left\{(\lambda_k^{(j)})^{-1/2}\beta_k^{(j)}\right\}_{k\in K^{(j)}} \xrightarrow{\text{SHT}} \{b_\ell^{(j)} a_{\ell m}\}_{\ell m} \xrightarrow{\times} \{\tilde{b}_\ell^{(j)} b_\ell^{(j)} a_{\ell m}\}_{\ell m} \xrightarrow{\text{SHT}^{-1}} \{\Psi^{(j)} X(\xi_k^{(j)})\}_{k\in K^{(j)}}$$

Standard pixelization packages, such as HEALPix, GLESP or SHTOOLS [2] come with optimized implementations of the direct and inverse Spherical Harmonic Transforms. For example, in the HEALPix scheme, pixels are located on rings of constant latitude, allowing for fast SHT. This makes the computation easy and tractable even at high resolution. The needlet coefficients at a given scale j can be visualized as a pixelized map. If the quadrature weights $\{\lambda_k^{(j)}\}$ are equal, the smoothed maps of Fig. 2, which are the outputs of the processing (14), provide a precise and easily interpretable picture of the space-frequency analysis.

Remark 1.7 *The quadrature points and weights* $\{(\xi_k^{(j)}, \lambda_k^{(j)})\}_{k\in K^{(j)}}$ *use to define the needlet coefficients* $\beta_k^{(j)}$ *and to sample the smoothed field* $\Psi^{(j)}X$ *may be*

[2] available at http://www.ipgp.jussieu.fr/∼wieczor/SHTOOLS/SHTOOLS.html

chosen identical to $\{(\xi_k, \lambda_k)\}_{k \in K}$ *used to sample the input field* X*. However, for data compression and computational efficiency, one can consider alternatively to take the minimal* $K^{(j)}$ *providing an exact positive-weight quadrature formula at a proper degree.*

2 Design of optimally localized wavelets

In this section, we define some criteria to compare the window profiles. Some of them are easily optimized, others are only investigated numerically. We first give some examples of generic needlet profiles we can think of (Section 2.1). Then, we restrict ourselves to a single scale j and an associated band $L := [\ell_{\min}, \ell_{\max}]$. The superscript (j) will be omitted in the notations when no confusion is possible. We present the $\mathbb{L}^2$ (Section 2.2) and statistical (Section 2.3) criteria, with practical implementation details on their optimizations.

2.1 Examples.

Narcowich et al. (2006) have derived the following theoretical bound that controls the decay of the needlets. In the B-adic case, if the function $\mathsf{b} := \sqrt{\mathsf{h}}$ defining the analysis spectral window is M-times continuously differentiable,

$$|\psi_k^{(j)}(\xi)| \leq \frac{C\ B^{j-1}}{1 + \left(B^{j-1} \arccos(\xi \cdot \xi_k^{(j)})\right)^M}$$

for some constant $C = C(\mathsf{b})$. This condition still allows a wide range of possibilities for designing the function b. Without restricting ourselves to the B-adic case, we implemented solutions to optimize in practice, non asymptotically, the shape of windows $b^{(j)}$ regarding some applications.

To illustrate the kind of aspects we are concerned with, we compare in Figure 4 the azimuthal profiles (in the spatial domain) of various axisymmetric needlets. The needlets are built from window functions $b^{(j)}$ via relation (9) and $\xi_k = (0, 0)$, *i.e.* they are centered on the North pole, and then are considered as functions of θ only. This illustration is restricted to the 9^{th} dyadic scale, *i.e.* frequencies in the band $L := [256, 1024]$. We shall compare heuristically five families of window functions. Note that the last two are not limited to band L.

(1) Square roots of splines of various orders. For any odd integer M, there exists a spline function h of order M, non-negative, compactly supported

on $[\frac{1}{2}, 2]$ and such that the $h_\ell^{(j)}$'s defined by (6) verify (5). It remains to define $b_\ell^{(j)} = \sqrt{h_\ell^{(j)}}$.

(2) Best concentrated Slepian functions in caps of various radii (cf Section 2.2). The window function $b_\ell^{(j)}$ is the minimizer of the criterion (20). It is band-limited on L and optimally concentrated in a polar cap $\Omega_{\theta_0} = \{\xi : \theta \leq \theta_0\})$, θ_0 being a free parameter.

(3) Denote G a primitive of the C^∞ function $g : x \mapsto e^{-\frac{1}{1-x^2}} 1_{(-1,1)}(x)$ and put

$$\mathsf{b}(x) = G(-8x + 3) - G(-4x + 3) \tag{15}$$

and $b_\ell^{(j)} = \mathsf{b}\left(\frac{\ell}{2^j}\right)$. This window function is used in Pietrobon et al. (2006).

(4) From the B-spline function of order 3

$$B_3(x) = \frac{1}{12}(|x-2|^3 - 4|x-1|^3 + 6|x|^3 - 4|x+1|^3 + |x+2|^3), \tag{16}$$

form $\mathsf{b}(x) = \frac{3}{2}(B_3(2x) - B_3(x))$ and define $b_\ell^{(j)} = \mathsf{b}\left(\frac{\ell}{2^j}\right)$. This window function is used by Starck et al. (2006).

(5) The Mexican hat wavelet on the sphere is the function the stereographic projection of which on the Euclidean plane is the usual Mexican hat wavelet. It has the following close expression depending on some positive scale parameter R

$$\psi_R(\theta) \propto (1 - 2R^2 \tan^2(\theta/2)) \exp\{-2R^2 \tan^2(\theta/2)\}. \tag{17}$$

This wavelet is popular in the astrophysics community (see *e.g.* González-Nuevo et al., 2006). We have chosen $R = 6.10^{-3}$ such that the spectral window is almost zero for $\ell > 1024$.

2.2 $\mathbb{L}^2$-concentration and variations

Our first attempt to achieve a good spatial localization of a needlet is to optimize a $\mathbb{L}^2$-norm based criterion, adapting to the sphere a problem that is well-known on the real line. In their seminal work in the 1960s and 1970s, Slepian and his collaborators studied the properties of prolate spheroidal wave functions (PSWFs) in the 1D case of real functions (see Slepian, 1983, and the references therein). PSWFs may be defined as functions with optimal energy concentration in the time domain, under some band-limitation constraint. Equivalently, they are the eigenfunctions of a time-frequency concentration kernel or the solutions of a Sturm-Liouville differential equation. The time-frequency concentration of PSWFs is understood in terms of continuous Fourier transform on $\mathbb{R}$. A discrete version of this theory, based on Fourier series coefficients, is derived in Slepian (1978).

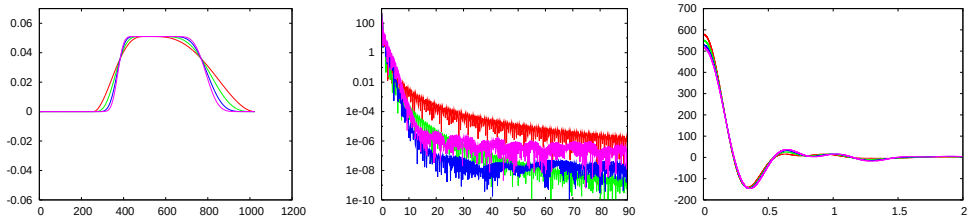

(a) Splines of order resp. 7, 15, 31 and 43.

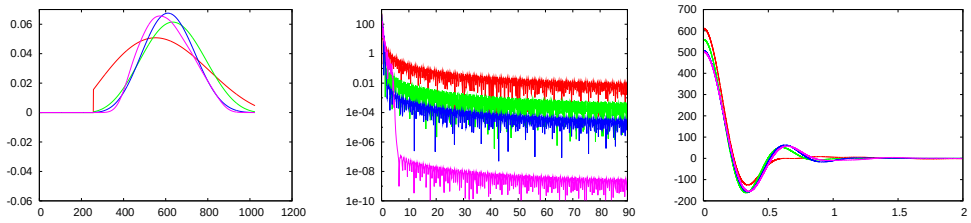

(b) PSWFs localized in polar caps of 0.5, 1, 1.5 and 5 degree opening

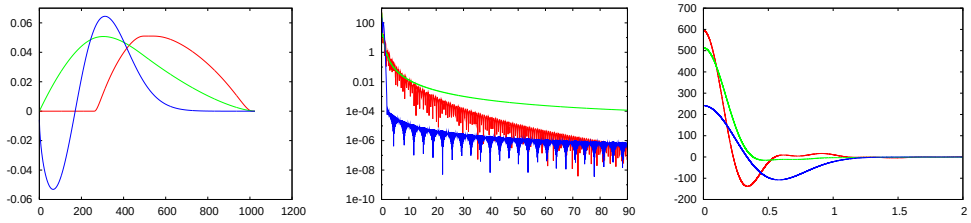

(c) (red curve) Exponential function described in Eq. (15), (green curve) B-spline function of Eq. (16) and (blue curve) Mexican hat described in Eq. (17).

Fig. 4. In left column, the shape of the spectral windows as a function of ℓ. In middle and right columns, the profile of the filters is plotted in the spatial domain as a function of θ (θ in degrees) with logarithmic and linear scales respectively, to illustrate both the decrease of the tail of the needlets far from the North pole and the shape of their first bounces.

In the last few years, Walter and coauthors exploited these 1D PSWFs to derive Slepian series (in Walter and Shen, 2003; see also Moore and Cada, 2004), and wavelets based on the best concentrated PSWF (Walter and Shen, 2004; Walter and Soleski, 2005).

On the sphere, we shall only consider the equivalent of Discrete PSWFs, following Simons et al. (2006). From a window function $\{b_\ell\}$ with support L,

define the axisymmetric function ψ by

$$\psi(\xi) = \sum_{\ell \in L} b_\ell L_\ell(\cos\theta). \tag{18}$$

The set of functions ψ of the form (18) is denoted $B_L \subset \mathbb{H}$. Given a spherical domain Ω, consider the minimization, among non-zero functions in B_L, of the criterion

$$\mathcal{C}_\Omega(\psi) = \frac{\int_{\mathbb{S}\setminus\Omega} \psi^2(\xi)\mathrm{d}\xi}{\int_{\mathbb{S}} \psi^2(\xi)\mathrm{d}\xi} = 1 - \frac{\int_{\Omega} \psi^2(\xi)\mathrm{d}\xi}{\int_{\mathbb{S}} \psi^2(\xi)\mathrm{d}\xi}. \tag{19}$$

This extension to the sphere of Slepian's concentration problem is studied in details by Simons et al. (2006) in the case $\ell_{\min} = 0$. We call PSWF (by abuse of language) and denote $\psi^\star_\Omega$ a normalized minimizer for $\mathcal{C}_\Omega(\psi)$.

The criterion (19) has a simplified expression when Ω is axisymmetric. Consider the polar cap $\Omega_{\theta_0} = \{\xi : \theta \leq \theta_0\}$ and define the coupling matrix $\mathbf{D} = (D_{\ell,\ell'})_{\ell,\ell' \in L}$ by

$$D_{\ell,\ell'} = \frac{8\pi^2}{\sqrt{(2\ell+1)(2\ell'+1)}} \int_{\cos\theta_0}^1 L_\ell(z) L_{\ell'}(z)\mathrm{d}z \ ,$$

and

$$\bar{\mathbf{b}}(\psi) = (\sqrt{\frac{2\ell_{\min}+1}{8\pi^2}} b_{\ell_{\min}}, \ldots, \sqrt{\frac{2\ell_{\max}+1}{8\pi^2}} b_{\ell_{\max}}).$$

Then

$$\mathcal{C}_\Omega(\psi) = 1 - \frac{\bar{\mathbf{b}}^t \mathbf{D} \bar{\mathbf{b}}}{\|\bar{\mathbf{b}}\|^2} \tag{20}$$

and the minimization of (19) becomes an eigenvalue problem. The solution of this minimization depends on the opening θ_0. In Figure 5 we plot the value of $\mathcal{C}_{\Omega_{\theta_0}}$ against θ_0 for $\psi^\star_{\Omega_{1^\circ}}, \psi^\star_{\Omega_{5^\circ}}, \psi^\star_{\Omega_{10^\circ}}$. The lowest curve is the minimum of the criterion for all openings θ_0. It is clear that there is no optimal function uniformly in θ_0: the concentration criterion $\mathcal{C}_{\Omega_0}$ of each PSWF $\psi^\star_{\Omega_{\theta_1}}$ reaches the best possible value for $\theta_0 = \theta_1$ only.

As in the 1-dimensional case, the spectrum of $\mathbf{D}$ exhibits a "step function" behaviour: denoting $N = \mathrm{tr}\ \mathbf{D}$ (the "Shannon number"), the matrix $\mathbf{D}$ has about N eigenvalues very close to 1, and most of the others close to zero (see Fig.6, and Simons et al. 2006 for details).

When several eigenvalues of $\mathbf{D}$ are extremely close to 1, it is computationally difficult to find the largest one and the associated eigenvector. In the case of Ω a polar cap and $\ell_{\min} = 0$, one can advantageously solve the less degenerated eigenvalue problem associated with the Grünbaum differential equation (Grünbaum et al., 1982) which has the same solutions as (19). We are not aware of an equivalent theory in the case $\ell_{\min} > 0$.

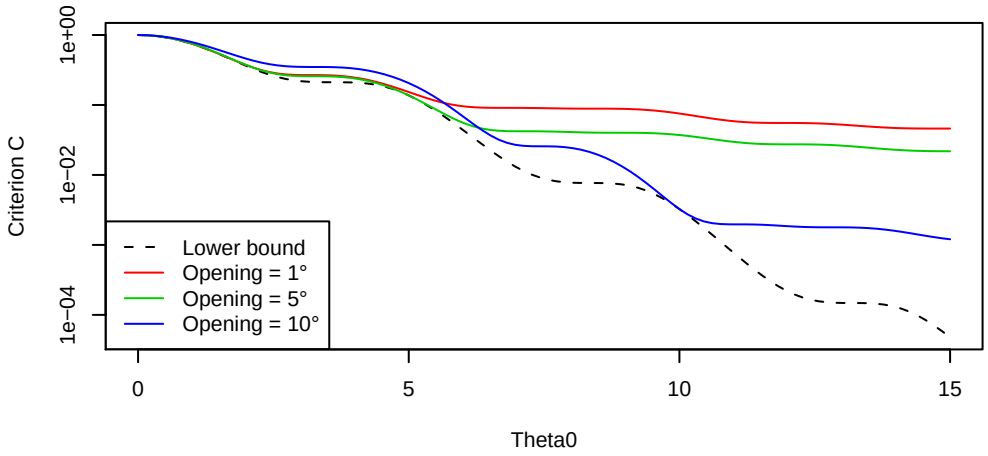

Fig. 5. Localization for $\mathbb{L}^2$-energy criterion of PSWFs, band-limited into $L = [33, 64]$. The dashed line is the minimum of the criterion $\mathcal{C}_{\Omega_{\theta_0}}$ as a function of θ_0 and the other ones are the values of $\mathcal{C}_{\Omega_{\theta_0}}(\psi)$ evaluated at $\psi = \psi^\star_{\Omega_1}$, $\psi^\star_{\Omega_5}$ and $\psi^\star_{\Omega_{10}}$.

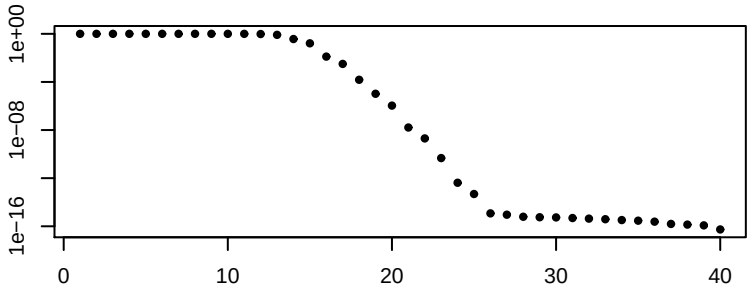

Fig. 6. Eigenvalues of matrix D with $\theta_0 = 50°$ and $L = [17, 64]$. In this case, Shannon number $N = 13.3$.

With ϵ being of the order the machine precision, all vectors in $V_\epsilon = \bigoplus_{\lambda \geq 1-\epsilon} \mathrm{Ker}(\mathbf{D} - \lambda \mathbf{Id})$ have well spatially localized counterparts, but they are not necessarily positive (in harmonic domain). This is not acceptable for instance if we were to use them as windows associated to smoothing operator (denoted h in the first Section), and implement this operator using a needlet analysis-synthesis scheme, the window of which has to be defined as the square-root of the PSWF's window. To circumvent this, we therefore introduce a modified coupling matrix $\widetilde{\mathbf{D}} = \mathbf{D} + a\mathbf{H}^t\mathbf{H}$ where $a > 0$ is a tuning parameter and $\mathbf{H}$ is the tridiagonal second-order finite difference matrix. Window functions are now obtained as minimizers of $\widetilde{\mathcal{C}_\Omega}(\psi) = 1 - \frac{\bar{\mathbf{b}}^t \widetilde{\mathbf{D}} \bar{\mathbf{b}}}{\|\mathbf{b}\|^2}$ instead of $\mathcal{C}_\Omega$. The additional term favors non-oscillating functions among the vectors of V_ϵ which are undistinguishable from their eigenvalues λ. Adding the "smoothing" term is expected not to alter the spatial localization of the filter. In practice, parameter a is selected to ensure 'computational uniqueness' of the smallest eigenvalue of $\widetilde{\mathbf{D}}$. Solutions obtained by the numerical implementation of the minimization of $\widetilde{\mathcal{C}_\Omega}$ are displayed in Figure 7, with various values for the smoothing pa-

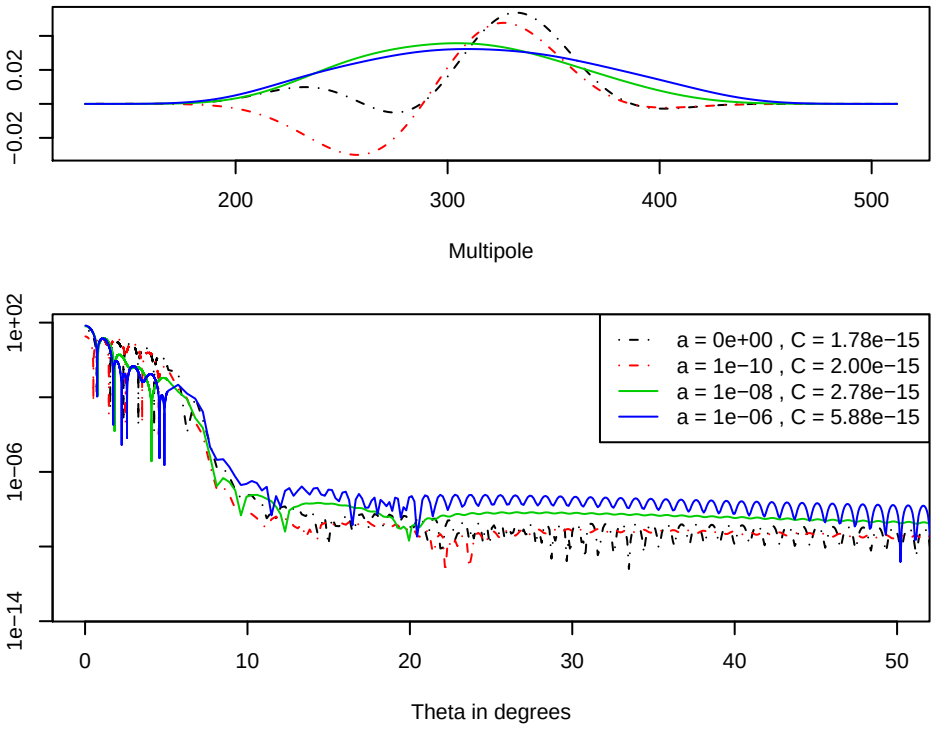

Fig. 7. Effect of the smoothing on the spectral and spatial shapes of PSWFs.

rameter a. Dashed lines correspond to the vector returned numerically as the "best" eigenvector of $\mathbf{D}$ (associated to the greatest eigenvalue), and the best eigenvector of $\tilde{\mathbf{D}}$ with parameter a chosen deliberately too small to ensure computationally uniqueness. Oscillating functions are indeed obtained. As a grows, the criterion selects non oscillating windows, two of which are shown by the plain lines. The loss measured by the increase of $\mathcal{C}_\Omega$ is displayed in the legend of the lower panel and appears extremely small. In our example, the energy outside Ω for the needlet built from $\tilde{\mathcal{C}}$ takes the value $2.78.10^{-15}$, whereas its minimal possible value is $1.78.10^{-15}$.

A generalization of the Slepian concentration problem can be to consider other measures of concentration, such as $\mathbb{L}^p$, $p = 1, ..., \infty$ instead of $\mathbb{L}^2$. The criterion defined in Eq. (19) becomes then

$$\mathcal{C}_\Omega^{(p)}(\psi) = 1 - \frac{\|\psi \mathbf{1}_\Omega\|_p^p}{\|\psi\|_p^p} \tag{21}$$

where $\|f\|_p^p = \int_{\mathbb{S}} |f(\xi)|^p \mathrm{d}\xi$ if $p \in [1, \infty)$ and $\|f\|_\infty^\infty = \operatorname{ess\,sup}_{\xi \in \mathbb{S}} |f(\xi)|$ for a spherical function f. Unlike Slepian criterion $\mathcal{C}_\Omega = \mathcal{C}_\Omega^{(2)}$, these alternate criteria do not lead to simple eigenvalue problems. They could be numerically optimized but this is beyond the scope of this paper. However we compare in Section 3.1 this criterion to the original one $\mathcal{C}_\Omega$.

Instead of focusing on the "geometrical" shape of the needlet, one may also optimize directly some alternate criterion of practical interest.

In this section, we consider the following framework: given an underlying random field X on $\mathbb{S}$ to be analysed, a window function W on $\mathbb{S}$ multiplying the field (for example a mask putting the field to zero in some regions) and a region $\mathbb{D} \subset \mathbb{S}$ of interest in which the analysis is to be done, the aim is to get, in $\mathbb{D}$, needlet coefficients of WX as close as possible to the coefficients computed from the uncorrupted field X.

We shall assume statistical properties on the fields X, W, D and look for optimality of the filters on average.

Assumption 2.1 *(1) X is a real-valued Gaussian zero mean isotropic square integrable random field on $\mathbb{S}$, with power spectrum (C_ℓ).*
(2) W and D are deterministic elements of $\mathbb{H}$.

Implicitly, X is a measurable mapping from some $(\mathcal{X}, \mathsf{X}, \mathbb{P})$ into $(\mathbb{H}, \mathsf{H})$, H being the Borel σ-filed of $\mathbb{H}$. Let $\mathbb{E}$ denote the expectation operator under $\mathbb{P}$. Recall that under Assumption 2.1, the covariance function on the field X is well defined and is given by

$$\mathbb{E}[X(\xi)X(\xi')] = (4\pi)^{-1} \sum_{\ell \in \mathbb{N}} C_\ell L_\ell(\xi \cdot \xi') \ .$$

It follows that $\mathbb{E}[X(\xi)^2] = (4\pi)^{-1} \sum_{\ell \in \mathbb{N}} (2\ell + 1) C_\ell$. Moreover, the multipole moments $(a_{\ell m})$ of X are complex Gaussian random variables. They are centered, independent up to the relation $a_{\ell m} = a^*_{\ell,-m}$ and satisfy $\mathbb{E}(|a_{\ell 0}|^2) = \frac{1}{2}\mathbb{E}(|a_{\ell m}|^2) = C_\ell$, $m \neq 0$.

Note that W and D can be indicator functions (binary *masks*) or any smooth functions on the sphere.

A first attempt in this direction is the derivation of an unbiased estimate of the spectrum from the multipole moments and the empirical power spectrum of the weighted sky XW defined by $\hat{a}_{\ell m} = \int_{\mathbb{S}} X(\xi) W(\xi) Y^*_{\ell m}(\xi) \mathrm{d}\xi$ and $\hat{C}_\ell = \frac{1}{2\ell+1} \sum_m \hat{a}^2_{\ell m}$ respectively. It is well-known (see Peebles, 1973; Hivon et al., 2002, see also the compact proof in Appendix A) that

$$\mathbb{E}(\hat{C}_\ell) = \sum_{\ell' \in \mathbb{N}} \mathcal{M}_{\ell\ell'} C_{\ell'} \text{ with } \mathcal{M}_{\ell\ell'} = \sum_{0 \leq \ell'' \leq \ell + \ell'} \alpha_{\ell\ell'\ell''} \frac{2\ell'' + 1}{2\ell + 1} C^W_{\ell''} \ , \qquad (22)$$

where the coefficients $\alpha_{\ell\ell'\ell''}$ are defined by (B.5). Note that the coupling matrix $\mathcal{M}$ depends on W only through its 'power spectrum' C^W_ℓ. If $\mathcal{M}$ is invertible,

then $(\mathcal{M}^{-1}(\hat{C}_{\ell'}))$ provides an unbiased estimate of (C_ℓ).

Let now derive a criterion to design a window function b which minimises the effect of missing data in a needlet analysis procedure. We focus on a single band smoothed field (*i.e.* we fix one scale j) and the dependence on j is implicit in the notations. For a collection of couple of indices, say $(\ell_i, m_i)_{i=1,\dots,I}$, we use $\sum^*_{(\ell_i,m_i)_{i=1,\cdots,I}}$ as a shorthand notation for the summation on $\ell_i \in \mathbb{N}, m_i \in \{-\ell_i, \cdots, \ell_i\}, i = 1, \dots, I$.

Given an analysis spectral window $\mathbf{b} = (b_{\ell_{\min}}, \cdots, b_{\ell_{\max}})$ and its associated smoothing operator $\Phi = \sum_{\ell_{\min} \le \ell \le \ell_{\max}} b_\ell \Pi_\ell$, the smoothed masked field is

$$\Phi XW(\xi) = \sum_{\ell \in L} b_\ell \int_{\mathbb{S}} X(\xi') W(\xi') L_\ell(\xi \cdot \xi') \mathrm{d}\xi'.$$

Write $\mathbb{E}[\Phi X(\xi)^2] = (4\pi)^{-1} \sum_\ell \sigma_\ell^2 b_\ell^2$ with $\sigma_\ell^2 = (2\ell+1)C_\ell$. Let ϵ denote the normalized difference field

$$\begin{aligned} \epsilon(\xi) &= \frac{\Phi X(\xi) - \Phi(XW)(\xi)}{\mathbb{E}^{1/2}[\Phi X(\xi)^2]} \\ &= \left(\sum \sigma_\ell^2 b_\ell^2\right)^{-1/2} \sum^*_{(l,m)} b_\ell \bar{a}_{\ell m} Y_{\ell m}(\xi) \end{aligned} \tag{23}$$

where we have defined $\bar{W} = 1 - W$, $\bar{a}_{\ell m} = \langle X\bar{W}, Y_{\ell m} \rangle$.

Suppose that $(\{(\xi_k\}_{k\in K}, \{\lambda_k)\}_{k\in K})$ provides an exact Gauss quadrature formula at a degree $2\ell_{\max}$. Define β_k and β'_k the needlet coefficients of X and XW, respectively and define

$$\epsilon_k = \frac{\beta_k - \beta'_k}{\sqrt{\mathbb{E}(\beta_k^2)}}.$$

Those random variables are normalized errors on the needlet coefficients induced by the application of the weight function W. If both X and XW are in $\mathbb{H}_{\ell_{\max}}$, we easily check that $\mathbb{E}(\beta_k^2) = \sqrt{\lambda_k}(4\pi)^{-1} \sum_\ell b_\ell^2 \sigma_\ell^2$ and

$$\forall k \in K,\ \epsilon_k = \epsilon(\xi_k)\ .$$

The dispersion of either the continuous field $\epsilon(\xi)$ or the finite set $\{\epsilon_k\}_{k\in K}$ is taken as a measure of quality for an analysis Φ. This dispersion is not measured on the whole sphere, since the difference ϵ must be important in the regions where W is far from 1. In order to select the regions where ϵ is to be minimized we introduce a function $D = \sum d_{\ell m} Y_{\ell m}$ which provides a positive weight function in $\mathbb{H}$. In the simplest case D can be $\mathbf{1}_{\mathbb{D}}$ for a region $\mathbb{D}$ of interest. More generally, D can be designed to give more or less importance to various regions of $\mathbb{S}$ according, for instance, to the need for reliability in the needlet coefficients.

The coefficients ϵ_k or their continuous version ϵ are used in two ways. The first one introduces a "tolerance" threshold α and counts the number of coefficients which are on average below this threshold. This measure of the efficiency of a filter in the presence of a mask is presented in Baldi et al. 2006; Pietrobon et al. 2006 but its optimization was not considered. The second one considers the integrated square error of ϵ, weighted by the function D. It leads to a quadratic quadratic which is readily optimized.

The first criterion, writes, for a binary function D,

$$E_{\mathbf{b}}(\alpha) = \frac{\sum_{k:D(\xi_k)=1} \mathbb{P}(|\epsilon_k| < \alpha)}{\sharp\{k : D(\xi_k) = 1\}}, \tag{24}$$

that is, the mean fraction of needlet coefficients corrupted by less than a normalized error $\alpha \geq 0$. For an arbitrary function D, a possible generalization of (24) is

$$E_{\mathbf{b}}(\alpha) = \frac{\sum_{k\in K} D(\xi_k)\mathbb{P}(|\epsilon_k| \leq \alpha)}{\sum_{k\in K} D(\xi_k)}.$$

In Subsection 3.2, we compare different windows using this criterion and a real mask.

Alternately, consider now the mean integrated square error (MISE)

$$R(\mathbf{b}) = \mathbb{E}\int_{\mathbb{S}} D(\xi)\|\epsilon(\xi)\|^2 \mathrm{d}\xi \tag{25}$$

and define the optimal shape for the window $\mathbf{b}$ as

$$\mathbf{b}^\star = \arg\min_{\|\mathbf{b}\|=1} R(\mathbf{b}). \tag{26}$$

Straightforward algebra leads to a close form expression of $R(\mathbf{b})$ depending on $\mathbf{b}$, on the weight functions W and D, and on the power spectrum $(C_\ell)_{\ell\in\mathbb{N}}$. Let $\bar{w}_{\ell m}, d_{\ell m}$ denote the multipole coefficients of the weight functions $\bar{W}, D$, respectively and

$$\begin{bmatrix} \ell & \ell' & \ell'' \\ m & m' & m'' \end{bmatrix} := \int_{\mathbb{S}} Y_{\ell m}(\xi) Y_{\ell' m'}(\xi) Y^*_{\ell'' m''}(\xi) \mathrm{d}\xi$$

(see (B.2) for an expression as a function of the Wigner-3j coefficients).

Proposition 2.2 *Under Assumption 2.1*

$$R(\mathbf{b}) = \frac{\mathbf{b}'\mathbf{Q}\mathbf{b}}{\mathbf{b}'\boldsymbol{\sigma}\mathbf{b}}$$

where $\boldsymbol{\sigma} = \mathrm{diag}((\sigma_\ell^2))$ *and* $\mathbf{Q}$ *is the matrix with entries*

$$Q_{\ell\ell'} = \sum_{m,m'} \sum\nolimits^*_{(\ell_1,m_1)} C_{\ell_1}$$
$$\sum\nolimits^*_{(\ell_i,m_i)_{i=2,3,4}} \bar{w}_{\ell_2 m_2} \bar{w}^*_{\ell_3 m_3} d_{\ell_4 m_4} \begin{bmatrix} \ell_1 & \ell_2 & \ell \\ m_1 & m_2 & m \end{bmatrix} \begin{bmatrix} \ell_1 & \ell_3 & \ell' \\ m_1 & m_3 & m' \end{bmatrix}^* \begin{bmatrix} \ell & \ell_4 & \ell' \\ m & m_4 & m' \end{bmatrix} . \quad (27)$$

If both W *and* D *are axisymmetric the ten-tuple summations above reduce to a five-tuple one*

$$\begin{aligned} Q_{\ell\ell'} &= \sum_m \sum_{\ell_1,\ell_2,\ell_3,\ell_4} C_{\ell_1} \bar{w}_{\ell_2 0} \bar{w}_{\ell_3 0} d_{\ell_4,0} \begin{bmatrix} \ell_1 & \ell_2 & \ell \\ m & 0 & m \end{bmatrix} \begin{bmatrix} \ell_1 & \ell_3 & \ell' \\ m & 0 & m \end{bmatrix} \begin{bmatrix} \ell & \ell_4 & \ell' \\ m & 0 & m \end{bmatrix} \\ &= \sum_m A_{\ell\ell' m} D_{\ell\ell' m} \ . \end{aligned}$$

In the next section we shall give some illustrative examples of optimal spectral windows $\mathbf{h}^\star$ in the particular axisymmetric case.

Remark 2.3 *As in the Slepian's problem, the design of an optimal filter reduces to an eigenvalue problem. In particular, if* $\sigma_\ell > 0$ *for any* $\ell \in L$*, write* $b^\dagger_\ell = \sigma_\ell b_\ell$*. Let* $\mathbf{b}^{\dagger\star}$ *be an eigenvector associated with the lowest eigenvalue of* $\mathbf{Q}^\dagger$*,* $Q^\dagger_{\ell\ell'} = (\sigma_\ell \sigma_{\ell'})^{-1} Q_{\ell\ell'}$*. Then* $\mathbf{b}^\star := \boldsymbol{\sigma}\tilde{\mathbf{b}}^{\dagger\star} / \|\boldsymbol{\sigma}\tilde{\mathbf{b}}^{\dagger\star}\|$ *is a solution of (26).*

Remark 2.4 *For those sums to be tractable, one has to assume that* D*,* W*,* C_ℓ *have finite support in the frequency domain,* i.e. *that the windows* D *and* W *are smooth (or apodized) and* $C_\ell = 0$ *for large enough* ℓ*.*

Remark 2.5 *The matrix* $\mathbf{Q}$ *being a second-order moment for the random field* X*, it can also be approximated by a moment estimator using Monte-Carlo experiments. This remark is of important practical interest as we are mostly concerned with non zonal masks.*

3 Examples, numerical results

3.1 Comparison of filters for various criteria

In Section 2, we considered several criteria measuring the localization properties of filters, and derived explicit or computational optimization for some of them. In Table 1, we compare the scores reached by the filters displayed in Figure 4. The columns indexed by $\mathbb{L}^2$-θ list the values $\mathcal{C}_{\Omega_\theta}(\psi)$ defined in

Eq. (19). More generally, the columns indexed by $\mathbb{L}^p$-θ correspond to the values $\mathcal{C}^p_{\Omega_\theta}(\psi)$ defined in Eq. (21). A column lists the values of $1 - E(\alpha)$ defined in Eq. (24), applied with the mask Kp0 of Fig. 8 and a tolerance parameter $\alpha = 10\%$ (see next subsection for more details). A last column gives, by way of illustration only, the value of the "uncertainty product" $\Delta_\xi(\psi) \times \Delta_{\mathsf{L}}(\psi)$, where

$$\Delta_\xi(\psi) = \frac{\sqrt{1 - \| \int_{\mathbb{S}} \xi\psi(\xi)^2 \mathrm{d}\xi \|^2}}{\int_{\mathbb{S}} \xi\psi(\xi)^2 \mathrm{d}\xi} \text{ and } \Delta_{\mathsf{L}}(\psi) = \sum_{\ell \geq 0} \ell(\ell+1) b_\ell^2. \qquad (28)$$

Narcowich and Ward (1996) proved that $\Delta_\xi(\psi) \times \Delta_{\mathsf{L}}(\psi) \geq 1$.

The PSWFs perform the best not only for the $\mathbb{L}^2$ criterion which they optimize, but also in most cases for the criteria where the $\mathbb{L}^2$ norm is replaced by $\mathbb{L}^p$ ones, $p = 1$ and $p = \infty$, with the same opening angles θ_0. Although the Kp0 mask has many small cut areas all over the sphere, most of the 11 filters presented here allow to retain more than 60% of the outside-mask coefficients β_k if a 10% error due to the presence of the mask is accepted. The performance w.r.t. this criterion goes up to 85% for the PSWF optimally concentrated in a cap of 1°. However, the choice of arbitrary value of α has a major impact on the ranking of the filters. This point is investigated in the next subsection.

3.2 Robustness of needlets coefficients

In this Subsection, we illustrate the performances of various window functions using the criterion (24). We have run $N = 30$ Monte-Carlo experiments to estimate the numerator of $E_{\mathbf{b}}(\alpha)$. The random fields X are drawn using the (C_ℓ)-spectrum of the best-fitting model for the CMB estimated by the WMAP team (Hinshaw et al., 2006). The mask W was chosen as Kp0, displayed in Figure 8, which masks the galactic plane and many point sources. The band is $L = [256, 1024]$.

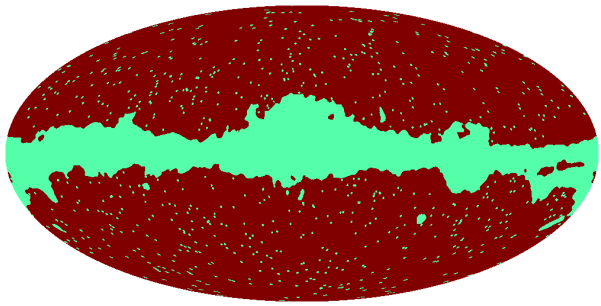

Fig. 8. Kp0 mask.

Figure 9 compares the increasing functions $E_{\mathbf{b}}(\cdot)$ corresponding to various filters $\mathbf{b}$. There is no "uniformly best" (*i.e.* highest in the figure) needlet:

	$\mathbb{L}^2$-0.5°	$\mathbb{L}^2$-1°	$\mathbb{L}^2$-1.5°	$\mathbb{L}^2$-5°	$\mathbb{L}^1$-0.5°	$\mathbb{L}^1$-1°	$\mathbb{L}^1$-1.5°	$\mathbb{L}^1$-5°	$\mathbb{L}^\infty$-0.5°	$\mathbb{L}^\infty$-1°	$\mathbb{L}^\infty$-1.5°	$\mathbb{L}^\infty$-5°	1-$E(0.1)$	$\Delta_\xi\Delta_\mathsf{L}$
Spline, order 3	2.2e-02	5.2e-03	7.4e-04	9.8e-07	4.2e-01	2.2e-01	1.0e-01	1.5e-02	5.0e-02	1.9e-02	5.1e-03	6.4e-05	2.6e-01	2.7
Spline, order 7	4.0e-02	1.3e-02	2.0e-03	4.8e-08	5.0e-01	2.9e-01	1.3e-01	1.7e-03	6.0e-02	2.7e-02	7.1e-03	1.2e-05	3.3e-01	3.1
Spline, order 15	6.1e-02	2.5e-02	4.9e-03	4.0e-07	5.9e-01	4.0e-01	2.2e-01	2.3e-03	6.9e-02	3.3e-02	9.8e-03	7.0e-05	4.1e-01	3.7
Spline, order 21	7.2e-02	3.1e-02	7.1e-03	7.7e-06	6.2e-01	4.5e-01	2.7e-01	1.0e-02	7.3e-02	3.7e-02	1.1e-02	2.7e-04	4.6e-01	4.1
Prolate, cap 0.5°	**1.2e-02**	6.0e-03	3.4e-03	9.5e-04	8.5e-01	8.2e-01	8.0e-01	7.2e-01	5.1e-02	1.0e-02	5.6e-03	1.0e-03	6.5e-01	9.8
Prolate, cap 1°	6.7e-02	**4.3e-05**	5.8e-06	1.7e-06	**3.8e-01**	1.3e-01	1.2e-01	1.1e-01	1.1e-01	**2.0e-03**	2.0e-04	5.0e-05	**1.5e-01**	3.1
Prolate, cap 1.5°	1.2e-01	1.5e-03	**3.4e-07**	1.2e-08	4.3e-01	**5.3e-02**	**1.0e-02**	8.8e-03	1.3e-01	1.7e-02	**1.4e-04**	4.5e-06	1.7e-01	3.6
Prolate, cap 5°	1.1e-01	6.7e-03	6.5e-04	**5.7e-14**	5.0e-01	1.8e-01	6.8e-02	**1.1e-06**	1.2e-01	2.2e-02	5.9e-03	**2.6e-08**	2.4e-01	3.6
Exponential	1.8e-02	3.2e-03	1.0e-03	1.0e-05	4.4e-01	2.6e-01	1.9e-01	4.8e-02	**4.4e-02**	1.4e-02	5.7e-03	1.9e-04	2.7e-01	**2.7**
B-Spline	**1.1e-02**	1.3e-03	3.9e-04	1.3e-05	4.8e-01	3.3e-01	2.7e-01	1.5e-01	**3.1e-02**	6.8e-03	2.5e-03	1.5e-04	2.1e-01	**1.2**
Mexican hat	6.4e-01	1.1e-02	8.5e-07	7.3e-12	7.9e-01	8.8e-02	**7.1e-04**	1.6e-04	4.7e-01	7.9e-02	4.5e-04	1.4e-07	4.9e-01	3.0

Table 1. Comparison of the eleven filters of Fig. 4, the nine first of which are band-limited in L=[256,1024].

some allow to retain more coefficients when the constraint imposed on the error is loose enough, but their efficiency decreases faster as α goes to zero. Inspect *e.g.* the PSWF family.

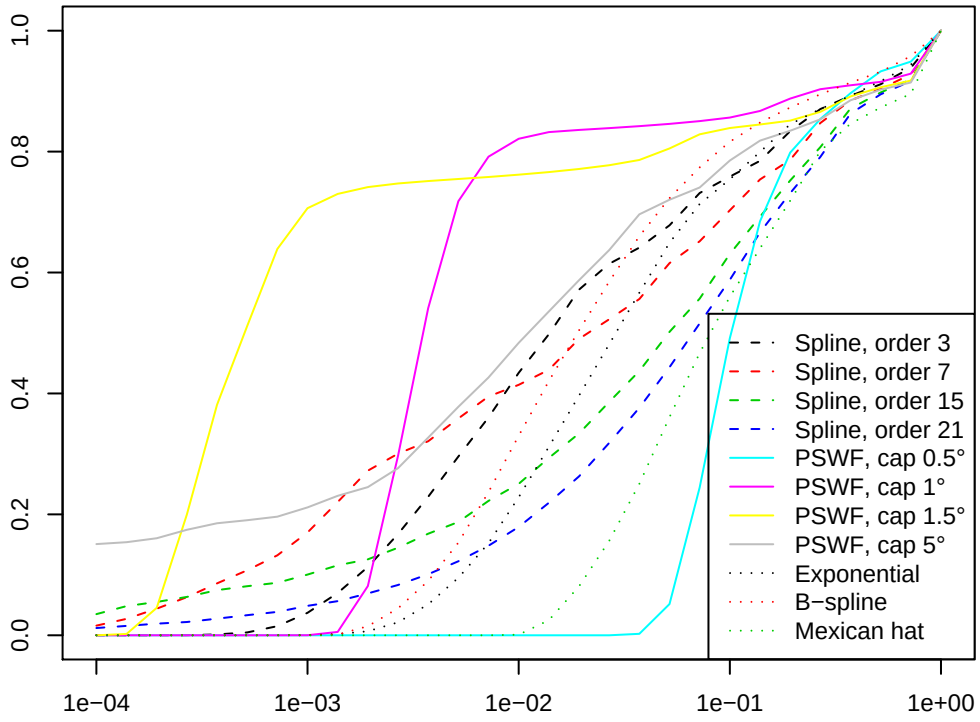

Fig. 9. Proportion $E_{\mathbf{b}}(\alpha)$ of coefficients uncontaminated at tolerance level α.

3.3 Some MISE-optimal filters for axisymmetric weight functions

We present here the results of the optimization (26) in the case of axisymmetric weight functions W. For simplicity, the reconstruction weight function D is taken equal to W. We stick to the CMB spectrum of previous subsection.

Figure 10 displays some of the masks W used in the experiments. The apodization in simply a cosine-arch junction between 0 and 1, on a 2-degrees angular range. This means that the data is available on the dark regions, and that its $L = [\ell_{\min}, \ell_{\max}]$-band-limited part has to be recovered in this area too.

On Figure 11 we have plotted the optimal filter in the $R(\mathbf{b})$-sense for the masks of Figure 10 together with different PSWFs. The criterion captures the symmetry of the mask (a) (the shape of the matrix $\mathbf{Q}$ is a "checkerboard"), and the optimal filter is thus zero on all even (here) or all odd multipoles. The associated axisymmetric needlet ψ is symmetric w.r.t. the equatorial plane, and thus is well concentrated around both the North and the South poles. Such solutions are very sensitive to the modifications of the masks.

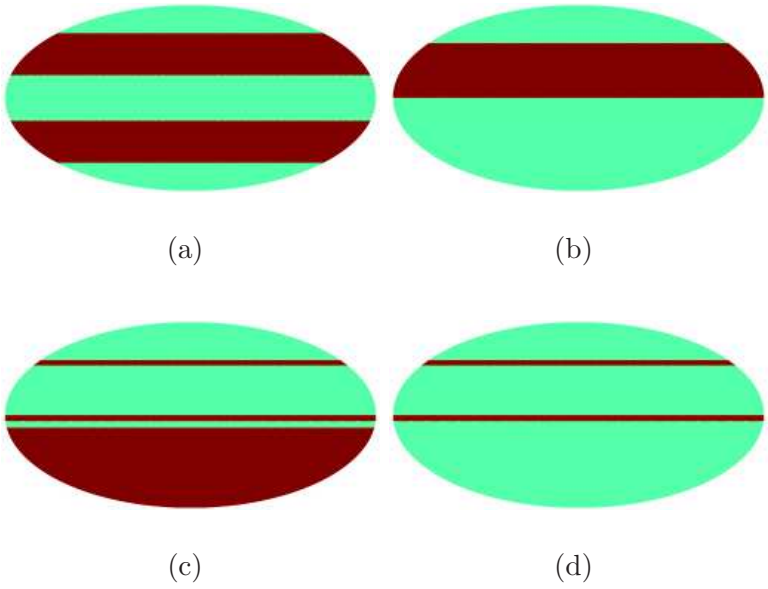

Fig. 10. Four different apodized masks. The degree of apodization, measured as the width of the cosine-arch 0-1 junction is, 2 degrees.

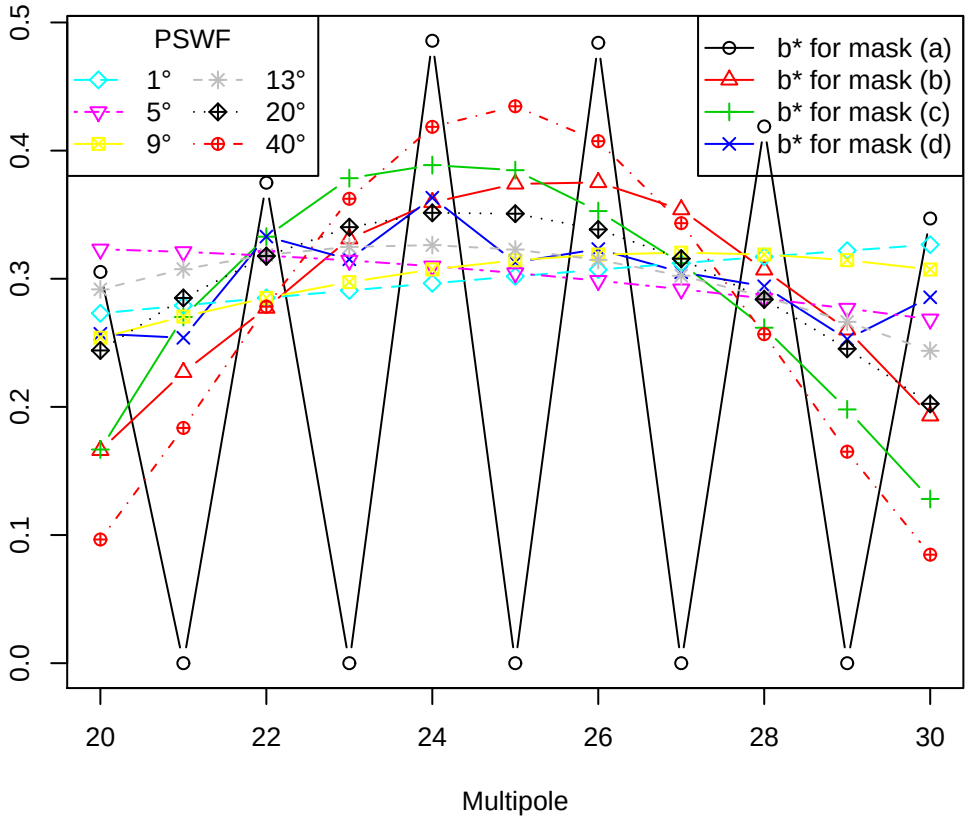

Fig. 11. Shape of optimal window functions (plain lines) and PSWF (coloured and dashed lines) with various openings.

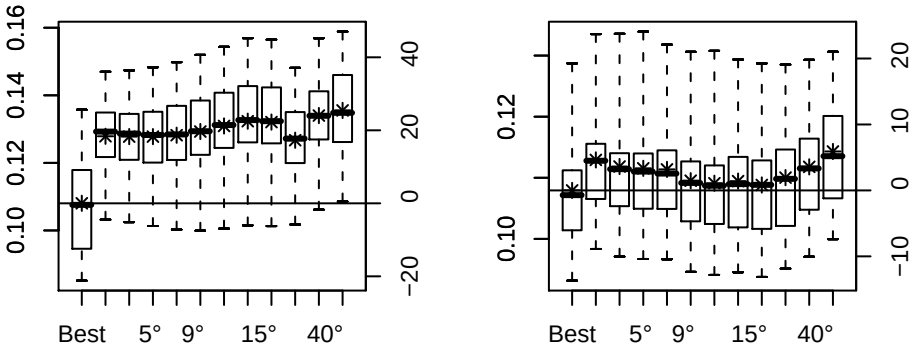

(a) (b)

Fig. 12. Mean square error in analysis. Stars are potted at the estimated values for $R(\mathbf{h})$. For Figure 12(a), the mask is Figure 10(a) and $L = [5, 15]$. For Figure 12(b), the mask is Figure 10 and $L = [20, 30]$

We conducted a small Monte-Carlo study to confirm the benefit of our approach. We have compared our best filters $\mathbf{b}^\star$ to PSWFs with different opening. On Figure 12, we show the box-plots of the distribution of the statistic $R(\mathbf{h})$ for all those filters. Stars are plotted at the position of the estimated value of $\mathbb{E}R(\mathbf{b})$ and the horizontal line is this value for $\mathbf{b}^\star$. The right vertical scale is for the relative error (in percent) with respect to $\mathbb{E}R(\mathbf{b}^\star)$.

Fig. 12(a) illustrates the strong benefit of a filter that captures the geometry of the mask. The relative improvement with respect to the best PSWF is of order 20%. It should be noted however that the shape of this optimal filter (described above) may lead to a misleading space-frequency picture. In some other cases, as shown in Figure 12(b), the relative improvement from the best PSWF to the best filter at all is very slight (a few percents). Here, the most favorable feature of our approach is that there is no tuning parameters (opening of the PSWF for instance, or the order of the splines window functions if they are taken as alternatives) to be found before the analysis.

4 Conclusion

A flexible way of analysing a field on the sphere in a space-frequency manner has been presented. It is based on the needlet construction of Narcowich et al. (2006). The proposed analysis functions form a frame in the space a square-integrable functions on the sphere. Decompositions are essentially operating in the Spherical Harmonics domain, leading to fast implementations. Various criteria are used to design good spectral windows. This optimization can lead to decisive improvement in high precision applications such as modern cosmol-

ogy (CMB spectral estimation, component separation, etc.), where localized analysis is crucial.

Acknowledgements

We wish to thank Jacques Delabrouille for fruitful discussions motivating this work for CMB analysis. Numerical work was conducted using HEALPix (Górski et al., 2005).

A Proofs

Proof of Propositions 1.4 and 1.5 Propositions 1.4 is a particular case of Proposition 1.5. Indeed (5)-(8) imply (12) with $C_1 = C_2 = 1$. Together with (10) we get $\tilde{\beta}_k^{(j)} = \beta_k^{(j)}$ and $\tilde{\psi}_k^{(j)} = \psi_k^{(j)}$. Prove now Proposition 1.5. Firstly, using successively (1) and the quadrature assumption (remind that for any $\ell, \ell' \leq d$, $(\Pi_\ell X)(\Pi_\ell X) \in \bigoplus_{l=0}^{2d} \mathbb{H}_l$)

$$\begin{aligned}
\sum_{j\in\mathcal{J}, k\in K^{(j)}} |\beta_k^{(j)}|^2 &= \sum_{j\in\mathcal{J}} \sum_{k\in K^{(j)}} \lambda_k^{(j)} \left| \sum_{\ell=0}^{d^{(j)}} b_\ell^{(j)} \int X(\xi) L_\ell(\xi \cdot \xi_k) \mathrm{d}\xi \right|^2 \\
&= \sum_{j\in\mathcal{J}} \sum_{k\in K^{(j)}} \lambda_k^{(j)} \left| \sum_{\ell=0}^{d^{(j)}} b_\ell^{(j)} \Pi_\ell X(\xi_k) \right|^2 \\
&= \sum_{j\in\mathcal{J}} \sum_{\ell,\ell'=0}^{d^{(j)}} b_\ell^{(j)} b_{\ell'}^{(j)} \sum_{k\in K^{(j)}} \lambda_k^{(j)} \Pi_\ell X(\xi_k) \Pi_{\ell'} X(\xi_k) \\
&= \sum_{j\in\mathcal{J}} \sum_{\ell,\ell'=0}^{d^{(j)}} b_\ell^{(j)} b_{\ell'}^{(j)} \int_{\mathbb{S}} \Pi_\ell X(\xi) \Pi_{\ell'} X(\xi) \mathrm{d}\xi \\
&= \sum_{j\in\mathcal{J}} \sum_{\ell,\ell'=0}^{d^{(j)}} b_\ell^{(j)} b_{\ell'}^{(j)} \delta_{\ell\ell'} \int_{\mathbb{S}} |\Pi_\ell X(\xi)|^2 \mathrm{d}\xi \\
&= \sum_{\ell\in\mathbb{N}} \sum_{j\in\mathcal{J}} (b_\ell^{(j)})^2 \|\Pi_\ell X\|^2 \,.
\end{aligned}$$

Using (12) and $\|X\|^2 = \sum_\ell \|\Pi_\ell X\|^2$, we get $C_1\|X\|^2 \leq \sum_{j,k} |\beta_k^{(j)}|^2 \leq C_2\|X\|^2$. Prove now that $(\tilde{\psi}_k^{(j)})$ is the dual frame of $(\psi_k^{(j)})$. Write

$$\begin{aligned}\langle \tilde{\psi}_{k'}^{(j')}, \psi_k^{(j)} \rangle &= (\lambda_{k'}^{(j')}\lambda_k^{(j)})^{(1/2)} \sum_{\ell'=0}^{d^{(j')}} \sum_{\ell=0}^{d^{(j)}} \tilde{b}_{\ell'}^{(j')} b_\ell^{(j)} \int_{\mathbb{S}} L_{\ell'}(\xi \cdot \xi_{k'}^{(j')}) L_\ell(\xi \cdot \xi_k^{(j)}) \mathrm{d}\xi \\ &= (\lambda_{k'}^{(j')}\lambda_k^{(j)})^{(1/2)} \sum_{\ell=0}^{d^{(j')}} \tilde{b}_\ell^{(j')} b_\ell^{(j)} L_\ell(\xi_{k'}^{(j')} \cdot \xi_k^{(j)})\end{aligned}$$

Then, for any $j \in \mathbb{N}$, $k \in K^{(j)}$

$$\begin{aligned}\sum_{j',k'} \langle \tilde{\psi}_k^{(j)}, \psi_{k'}^{(j')} \rangle \psi_{k'}^{(j')} &= (\lambda_k^{(j)})^{1/2} \sum_{j',k'} \lambda_{k'}^{(j')} \sum_{\ell=0}^{d^{(j')}} \tilde{b}_\ell^{(j')} b_\ell^{(j)} L_\ell(\xi_{k'}^{(j')} \cdot \xi_k^{(j)}) \sum_{\ell'=0}^{d^{(j')}} b_{\ell'}^{(j')} L_{\ell'}(\xi_{k'}^{(j')} \cdot \xi) \\ &= (\lambda_k^{(j)})^{1/2} \sum_{j' \in \mathcal{J}} \sum_{\ell=0}^{d^{(j')}} \tilde{b}_\ell^{(j')} b_\ell^{(j)} \sum_{\ell'=0}^{d^{(j')}} b_{\ell'}^{(j')} \sum_{k' \in K^{(j)}} \lambda_{k'}^{(j')} L_\ell(\xi_{k'}^{(j')} \cdot \xi_k^{(j)}) L_{\ell'}(\xi_{k'}^{(j')} \cdot \xi) \\ &= (\lambda_k^{(j)})^{1/2} \sum_{j' \in \mathcal{J}} \sum_{\ell=0}^{d^{(j')}} \tilde{b}_\ell^{(j')} b_\ell^{(j)} \sum_{\ell'=0}^{d^{(j')}} b_{\ell'}^{(j')} \int_{\mathbb{S}} L_\ell(\xi' \cdot \xi_k^{(j)}) L_{\ell'}(\xi' \cdot \xi) \mathrm{d}\xi' \\ &= (\lambda_k^{(j)})^{1/2} \sum_{j' \in \mathcal{J}} \sum_{\ell=0}^{d^{(j')}} \tilde{b}_\ell^{(j')} b_\ell^{(j)} \sum_{\ell'=0}^{d^{(j')}} b_{\ell'}^{(j')} \delta_{\ell\ell'} L(\xi_k^{(j)} \cdot \xi) \\ &= (\lambda_k^{(j)})^{1/2} \sum_{\ell=0}^{\infty} b_\ell^{(j)} \sum_{j' \in \mathcal{J}} \tilde{b}_\ell^{(j')} b_\ell^{(j')} L(\xi_k^{(j)} \cdot \xi) \\ &= \psi_k^{(j)} \ .\end{aligned}$$

The assertions (13) are a consequence of the dual frame property (see *e.g.* Daubechies, 1992).

Proof of Proposition 1.6 From Definition 1.3 of ψ_k and Eq (1)

$$\beta_k = \langle X, \psi_k \rangle = \sqrt{\lambda_k} \sum_\ell b_\ell \int_{\mathbb{S}} X(\xi) L_\ell(\xi, \xi_k) \mathrm{d}\xi = \sqrt{\lambda_k} \Phi X(\xi_k). \qquad \square$$

Proof of Eq. (22)

$$
\begin{aligned}
(2\ell+1)\mathbb{E}(\hat{C}_\ell) &= \sum_{m=-\ell}^{\ell} \iint_{\mathbb{S}\times\mathbb{S}} \mathbb{E}\left\{X(\xi)X(\xi')\right\} Y_{\ell m}(\xi)Y_{\ell m}(\xi')W(\xi)W(\xi')\mathrm{d}\xi\mathrm{d}\xi' \\
&= \iint_{\mathbb{S}\times\mathbb{S}} \Big\{\sum_{\ell'\in\mathbb{N}} C_{\ell'}L_{\ell'}(\xi\cdot\xi')\Big\} L_\ell(\xi\cdot\xi')W(\xi)W(\xi')\mathrm{d}\xi\mathrm{d}\xi' \\
&= \sum_{\ell'\in\mathbb{N}} C_{\ell'} \sum_{0\le\ell''\le\ell+\ell'} \alpha_{\ell\ell'\ell''} \iint_{\mathbb{S}\times\mathbb{S}} L_{\ell''}(\xi\cdot\xi')W(\xi)W(\xi')\mathrm{d}\xi\mathrm{d}\xi' \\
&= \sum_{\ell'\in\mathbb{N}} C_{\ell'} \sum_{0\le\ell''\le\ell+\ell'} \alpha_{\ell\ell'\ell''}(2\ell''+1)C^W_{\ell''}
\end{aligned}
$$

Proof of Proposition 2.2 As $X\bar{W} = \sum^*_{(\ell_1,m_1)} a_{\ell_1 m_1} Y_{\ell_1 m_1} \sum^*_{(\ell_2,m_2)} \bar{w}_{\ell_2 m_2} Y_{\ell_2 m_2}$,

$$
\bar{a}_{\ell m} := \langle X\bar{W}, Y_{\ell m}\rangle = \sum\nolimits^*_{(\ell_i,m_i)_{i=1,2}} a_{\ell_1 m_1}\bar{w}_{\ell_2 m_2} \begin{bmatrix} \ell_1 & \ell_2 & \ell \\ m_1 & m_2 & m \end{bmatrix}.
$$

Together with $\mathbb{E}[a_{\ell m}a^*_{\ell' m'}] = C_\ell \delta_{\ell\ell'}\delta_{mm'}$ it yields

$$
\mathbb{E}[\bar{a}_{\ell m}\bar{a}^*_{\ell' m'}] = \sum\nolimits^*_{(\ell_i,m_i)_{i=1,2,3}} C_{\ell_1}\bar{w}_{\ell_2 m_2}\bar{w}^*_{\ell_3 m_3} \begin{bmatrix} \ell_1 & \ell_2 & \ell \\ m_1 & m_2 & m \end{bmatrix} \begin{bmatrix} \ell_1 & \ell_3 & \ell' \\ m_1 & m_3 & m' \end{bmatrix}^* \quad \text{(A.1)}
$$

Combining (23) and (A.1) we get

$$
\begin{aligned}
R(\mathbf{b}) &= (\sum_{\ell\in\mathbb{N}} \sigma^2_\ell h^2_\ell)^{-1}\mathbb{E}\int_{\mathbb{S}} \sum\nolimits^*_{(\ell_4,m_4)} d_{\ell_4 m_4} Y_{\ell_4 m_4}(\xi) \left|\sum\nolimits^*_{(l,m)} h_\ell \bar{a}_{\ell m} Y_{\ell m}(\xi)\right|^2 \mathrm{d}\xi \\
&= (\sum_{\ell\in\mathbb{N}} \sigma^2_\ell h^2_\ell)^{-1} \sum_{\ell,\ell'\in\mathbb{N}} h_\ell h_{\ell'} \sum_{mm'} \mathbb{E}[\bar{a}_{\ell m}\bar{a}^*_{\ell' m'}] \sum\nolimits^*_{(\ell_4,m_4)} d_{\ell_4 m_4} \int_{\mathbb{S}} Y_{\ell_4 m_4}(\xi)Y_{\ell m}(\xi)Y^*_{\ell' m'}(\xi)\mathrm{d}\xi \\
&= (\sum_{\ell\in\mathbb{N}} \sigma^2_\ell h^2_\ell)^{-1} \sum_{\ell,\ell'\in\mathbb{N}} h_\ell h_{\ell'} Q_{\ell\ell'}.
\end{aligned}
$$

If W is axisymmetric,

$$
\begin{aligned}
\mathbb{E}[\bar{a}_{\ell m}\bar{a}^*_{\ell' m'}] &= \sum\nolimits^*_{\ell_1,m_1} C_{\ell_1} \sum_{\ell_2,\ell_3} \bar{w}_{\ell_2 0}\bar{w}_{\ell_3 0} \begin{bmatrix} \ell_1 & \ell_2 & \ell \\ m_1 & 0 & m \end{bmatrix} \begin{bmatrix} \ell_1 & \ell_3 & \ell' \\ m_1 & 0 & m' \end{bmatrix} \\
&= \delta_{m,m'} \sum_{\ell_1,\ell_2,\ell_3} C_{\ell_1}\bar{w}_{\ell_2 0}\bar{w}_{\ell_3 0} \begin{bmatrix} \ell_1 & \ell_2 & \ell \\ m & 0 & m \end{bmatrix} \begin{bmatrix} \ell_1 & \ell_3 & \ell' \\ m & 0 & m \end{bmatrix} =: A_{\ell\ell' m} \quad \text{(A.2)}
\end{aligned}
$$

where we used the fact that $\begin{bmatrix} \ell & \ell' & \ell'' \\ m & 0 & m'' \end{bmatrix} = 0$ if $m \neq m''$ and that $w_{l_3 0}$ and $\begin{bmatrix} \ell_1 & \ell_2 & \ell \\ m & 0 & m \end{bmatrix}$ are real. If D is axisymmetric and with $D_{\ell\ell' m} := \sum_{\ell_4} d_{\ell_4,0} \begin{bmatrix} \ell & \ell_4 & \ell' \\ m & 0 & m \end{bmatrix}$

$$Q_{\ell\ell'} = \sum_m \sum_{(\ell_i, m_i)_{i=1,2,3}} C_{\ell_1} \bar{w}_{\ell_2 m_2} \bar{w}^*_{\ell_3 m_3} \begin{bmatrix} \ell_1 & \ell_2 & \ell \\ m_1 & m_2 & m \end{bmatrix} \begin{bmatrix} \ell_1 & \ell_3 & \ell' \\ m_1 & m_2 & m \end{bmatrix}^* \sum_{\ell_4 \in \mathbb{N}} d_{\ell_4 0} \begin{bmatrix} \ell & \ell_4 & \ell' \\ m & 0 & m \end{bmatrix}. \qquad \square$$

B Legendre polynomials, spherical harmonics and related useful formulae

Usually, $P_\ell(z)$ denotes the Legendre polynomial of order ℓ, normalized by $P_\ell(1) = 1$. For our purposes, it is more convenient to use a different normalization

$$L_\ell(z) = \frac{2\ell + 1}{4\pi} P_\ell(z)$$

because we get coefficient-free properties like

$$L_\ell(\xi' \cdot \xi) = \sum_{m=-\ell}^{\ell} Y^*_{\ell m}(\xi) Y_{\ell m}(\xi')$$

and

$$\int_{\mathbb{S}} L_\ell(\eta \cdot \xi) L_{\ell'}(\eta' \cdot \xi) \mathrm{d}\xi = \delta_{\ell\ell'} L_\ell(\eta \cdot \eta'). \tag{B.1}$$

In other words, L_ℓ is the polynomial kernel of the harmonic projection on $\mathbb{H}_\ell$. We have $\int_{-1}^{+1} P_\ell(z)^2 \mathrm{d}z = \frac{2}{2\ell+1}$ and $\int_{-1}^{+1} L_\ell(z)^2 \mathrm{d}z = \frac{2\ell+1}{8\pi^2}$.

The spherical harmonics are explicitly given in a factorized form in terms of the associated Legendre polynomials and the complex exponentials as

$$Y_{\ell m}(\theta, \varphi) = \sqrt{\frac{(2\ell+1)}{4\pi} \frac{(\ell - m)!}{(\ell + m)!}} P_{\ell m}(\cos\theta) e^{im\varphi}$$

where $P_{\ell m}(x) = (-1)^m (1 - x^2)^{m/2} \frac{\mathrm{d}^m}{\mathrm{d}x^m} P_\ell(x)$.

The following equations relate the integral of the product of three complex spherical harmonics over the total solid angle or three Legendre polynomials with the Wigner-3j coefficients (for a definition in terms of Clebsh-Gordan

coefficients, see Varshalovich et al. (1988), pp235–).

$$\begin{aligned}\begin{bmatrix} \ell_1 & \ell_2 & \ell_3 \\ m_1 & m_2 & m_3 \end{bmatrix} &= \int_{\mathbb{S}} Y_{\ell_1 m_1}(\xi) Y_{\ell_2 m_2}(\xi) Y^*_{\ell_3 m_3}(\xi) \mathrm{d}\xi \\ &= (-1)^{m_3} \int_{\mathbb{S}} Y_{\ell_1 m_1}(\xi) Y_{\ell_2 m_2}(\xi) Y_{\ell_3 -m_3}(\xi) \mathrm{d}\xi \\ &= (-1)^{m_3} \sqrt{\frac{(2\ell_1+1)(2\ell_2+1)(2\ell_3+1)}{4\pi}} \begin{pmatrix} \ell_1 & \ell_2 & \ell_3 \\ 0 & 0 & 0 \end{pmatrix} \begin{pmatrix} \ell_1 & \ell_2 & \ell_3 \\ m_1 & m_2 & -m_3 \end{pmatrix} \end{aligned} \tag{B.2}$$

$$\frac{1}{2} \int L_\ell(z) L_{\ell'}(z') L_{\ell''}(z'') \mathrm{d}z \mathrm{d}z' \mathrm{d}z'' = \frac{(2\ell+1)(2\ell'+1)(2\ell''+1)}{(4\pi)^3} \begin{pmatrix} \ell & \ell' & \ell'' \\ 0 & 0 & 0 \end{pmatrix}^2 \tag{B.3}$$

$$= (4\pi)^{-2} \begin{bmatrix} \ell_1 & \ell_2 & \ell_3 \\ 0 & 0 & 0 \end{bmatrix} \tag{B.4}$$

From (B.3) and $\int L_\ell L_{\ell'} = \delta_{\ell,\ell'} \frac{2\ell+1}{8\pi^2}$ we get:

$$L_\ell L_{\ell'} = \sum_{0 \le \ell'' \le \ell+\ell'} \alpha_{\ell\ell'\ell''} L_{\ell''}$$

with

$$\alpha_{\ell\ell'\ell''} = \frac{(2\ell+1)(2\ell'+1)}{4\pi} \begin{pmatrix} \ell & \ell' & \ell'' \\ 0 & 0 & 0 \end{pmatrix}^2 . \tag{B.5}$$

References

Antoine, J.-P., Vandergheynst, P., 1999. Wavelets on the 2-sphere: a group-theoretical approach. Appl. Comput. Harmon. Anal. 7 (3), 262–291.

Baldi, P., Kerkyacharian, G., Marinucci, D., Picard, D., 2006. Asymptotics for spherical needlets, on arXiv.org : math.ST/0606599.

Bogdanova, I., Vandergheynst, P., Antoine, J.-P., Jacques, L., Morvidone, M., 2005. Stereographic wavelet frames on the sphere. Appl. Comput. Harmon. Anal. 19 (2), 223–252.

Dahlke, S., Dahmen, W., Weinreich, I., Schmitt, E., 1995. Multiresolution analysis and wavelets on S^2 and S^3. Numer. Funct. Anal. Optim. 16 (1-2), 19–41.

Daubechies, I., 1992. Ten lectures on wavelets. Vol. 61 of CBMS-NSF Regional Conference Series in Applied Mathematics. Society for Industrial and Applied Mathematics (SIAM), Philadelphia, PA.

Doroshkevich, A., Naselsky, P., Verkhodanov, O., Novikov, D., Turchaninov, V., Novikov, I., Christensen, P., Chiang, L., 2005. Gauss–Legendre Sky Pixelization (GLESP) for CMB maps. Int. J. of Modern Physics D 14, 275.

Freeden, W., Windheuser, U., 1997. Combined spherical harmonic and wavelet expansion — A future concept in Earth's gravitational determination. Appl. Comput. Harmon. Anal. 4, 1–37.

González-Nuevo, J., Argüeso, F., López-Caniego, M., Toffolatti, L., Sanz, J., Vielva, P., Herranz, D., 2006. The Mexican hat wavelet family: application to point-source detection in cosmic microwave background maps. Mon. Not. Roy. Astron. Soc. 369, 1603–1610.

Górski, K., Hivon, E., Banday, A., Wandelt, B., Hansen, F., Reinecke, M., Bartelmann, M., Apr. 2005. HEALPix: A Framework for High-Resolution Discretization and Fast Analysis of Data Distributed on the Sphere. Astrophys. J. 622, 759–771.

Grünbaum, F. A., Longhi, L., Perlstadt, M., 1982. Differential operators commuting with finite convolution integral operators: some nonabelian examples. SIAM J. Appl. Math. 42 (5), 941–955.

Hinshaw, G., Nolta, M., Bennett, C., Bean, R., Dore, O., Greason, M., Halpern, M., Hill, R., Jarosik, N., Kogut, A., Komatsu, E., Limon, M., Odegard, N., Meyer, S., Page, L., Peiris, H., Spergel, D., Tucker, G., Verde, L., Weiland, J., Wollack, E., Wright, E., 2006. Three-Year Wilkinson Microwave Anisotropy Probe (WMAP) Observations: Temperature Analysis. On arXiv.org: astro-ph/0603451.

Hivon, E., Górski, K., Netterfield, C., Crill, B., Prunet, S., Hansen, F., 2002. MASTER of the cosmic microwave background anisotropy power spectrum: A fast method for statistical analysis of large and complex cosmic microwave background data sets. Astrophys. J. 567, 2–17.

Holschneider, M., Chambodut, A., Mandea, M., 2003. From global to regional analysis of the magnetic field on the sphere using wavelet frames. Physics of the Earth and Planetary Interiors 135, 107–124(18).

McEwen, J., Vielva, P., Barreiro, R., Calyon, L., Hobson, M., Lazenby, A., Martinez-Gonzalez, E., Sanz, J., 2007. Cosmological applications of a wavelet analysis on the sphere. To appear.

Moore, I., Cada, M., 2004. Prolate spheroidal wave functions, an introduction to the slepian series and its properties. Appl. Comput. Harmon. Anal. 16, 208–230.

Narcowich, F., Petrushev, P., Ward, J., 2006). Localized tight frames on spheres. SIAM J. Math. Anal. 38 (2), 574–594.

Narcowich, F., Ward, J., 1996. Nonstationary wavelets on the m-sphere for scattered data. Appl. Comput. Harm. Anal. 3, 324–336.

Peebles, P. J. E., 1973. Statistical analysis of catalogs of extragalactic objects. I. Theory. Astrophys. J. 185, 413–440.

Pietrobon, D., Balbi, A., Marinucci, D., 2006. Integrated Sachs-Wolfe effect from the cross correlation of WMAP3 year and the NRAO VLA sky survey data: New results and constraints on dark energy. Phys. Rev. D 74.

Potts, D., Tasche, M., 1995. Interpolatory wavelets on the sphere. In: Chui, C., Schumaker, L. (Eds.), Approximation Theory VIII, Vol. 2: Wavelets. World Scientific, pp. 335–342.

Schröder, P., Sweldens, W., 1995. Spherical wavelets: Efficiently representing functions on the sphere. Computer Graphics Proceedings (SIGGRAPH 95) , 161–172.

Simons, F., Dahlen, F., Wieczorek, M., 2006. Spatiospectral concentration on a sphere. SIAM Rev. 48 (504).

Slepian, D., May-June 1978. Prolate spheroidal wave functions, Fourier analysis and uncertainty — V: The discrete case. Bell Syst. Tech. J. 57, 1371–1429.

Slepian, D., 1983. Some comments on Fourier analysis, uncertainty and modeling. SIAM Rev. 25 (3), 379–393.

Starck, J.-L., Moudden, Y., Abrial, P., Nguyen, M., 2006. Wavelets, ridgelets and curvelets on the sphere. Astronomy & Astrophysics 446, 1191–1204.

Torresani, B., 1995. Position-frequency analysis for signals defined on spheres. Signal Process. 43 (3), 341–346.

Varshalovich, D., Moskalev, A., Khersonskiĭ, V., 1988. Quantum theory of angular momentum. World Scientific Publishing Co. Inc.

Vielva, P., Martinez-Gonzalez, E., Barreiro, R., Sanz, J., Cayon, L., 2004. Detection of non-Gaussianity in the WMAP 1-year data using spherical wavelets. Astrophys. J. 609, 22.

Walter, G., Shen, X., Jan. 2003. Sampling with prolate spheroidal wave functions. Sampl. Theory Signal Image Process. 2 (1), 25–52.

Walter, G., Shen, X., 2004. Wavelets based on prolate spheroidal wave functions. J. Fourier Anal. Appl. 10 (1), 1–26.

Walter, G., Soleski, T., 2005. A new friendly method of computing prolate spheroidal wave functions and wavelets. Appl. Comput. Harmon. Anal. 19, 432–443.

Wiaux, Y., Jacques, L., Vandergheynst, P., 2005. Correspondence principle between spherical and euclidean wavelets. Astrophys. J. 632, 15.

Wieczorek, M., Simons, F., 2005. Localized spectral analysis on the sphere. Geophys. J. Int. 162 (3), 655–675.